Combustion and Flame 162 (2015) 2231–2247

Contents lists available at ScienceDirect

Combustion and Flame

journal homepage: www.elsevier.com/locate/combustflame

Numerical and experimental study of the influence of CO_2 and N_2 dilution on soot formation in laminar coflow C_2H_4/air diffusion flames at pressures between 5 and 20 atm

Fengshan Liu [a,*], Ahmet E. Karataş [b], Ömer L. Gülder [b], Mingyan Gu [c]

[a] Black Carbon Metrology, Measurement Science and Standards, National Research Council, 1200 Montreal Road, Ottawa, Ontario K1A 0R6, Canada
[b] Institute for Aerospace Studies, University of Toronto, 4925 Dufferin Street, Toronto, Ontario M3H 5T6, Canada
[c] School of Energy and Environment, Anhui University of Technology, Ma'anshan 243002, China

ARTICLE INFO

Article history:
Received 21 October 2014
Received in revised form 24 January 2015
Accepted 26 January 2015
Available online 19 February 2015

Keywords:
Soot formation
Laminar diffusion flame
Pressure effect
CO_2 chemical effect

ABSTRACT

The effects of fuel dilution by CO_2 and N_2 on soot formation and the flame structure in laminar coflow C_2H_4/air diffusion flames at pressures between 5 and 20 atm were investigated both experimentally and numerically. Experimentally a constant ethylene flow rate and a constant dilution rate of 1:2 (fuel:diluent by mass) were maintained throughout the experiments. The flames were stable and non-smoking over the pressure range investigated. The radially-resolved soot volume fraction and temperature distributions were measured by the spectral soot emission (SSE) technique. Numerical calculations were conducted using two C_2 chemistry models with formation of PAHs up to pyrene and a soot model incorporating pyrene collision as the soot inception step and hydrogen-abstraction acetylene addition mechanism and PAH condensation as the surface growth processes. The two C_2 chemistry models were the ABF mechanism [Appel et al. (2000)] and the DLR mechanism [Slavinskaya and Frank (2009)]. The DLR mechanism predicted little or no chemical effect of CO_2 dilution, depending on the pressure, in the present context. Numerical results are in qualitative agreement with experimental measurements. Soot volume fractions and carbon conversion are lower in the CO_2-diluted flames due to the additional chemical effect of CO_2. CO_2 is still more effective than N_2 as a diluent to suppress soot formation at elevated pressures. The primary pathway for the chemical effect of CO_2 dilution is through the reverse reaction of $CO + OH \leftrightarrow CO_2 + H$. The chemical effect of CO_2 lowers the rates of soot inception, C_2H_2 addition, and PAH condensation. The effectiveness of the CO_2 chemical effect on soot formation suppression diminishes with increasing pressure. The diminishing effectiveness of the chemical effect of CO_2 dilution with increasing pressure is due to the significant decrease in the H radical mole fraction.

1. Introduction

Soot is formed during incomplete combustion of hydrocarbons and is the most efficient light-absorbing nano-aerosol, absorbing orders of magnitude more energy by mass than CO_2. Soot particles emitted from various combustion systems have been identified to be a key contributor to global warming [1] and found harmful to human health [2]. Development of effective combustion and/or fuel technologies to reduce soot emissions from combustion devices has been an active research topic over the last several decades.

In response to the increasingly more stringent regulations of pollutant emissions (NOx and soot) various low-temperature combustion technologies have been developed to reduce both NOx and soot emissions. The common feature of these technologies is to dilute the fuel and/or the oxidizer stream with the combustion products to achieve lean-burn conditions. This technology is called exhaust gas recirculation (EGR) in diesel and gasoline engines, while it is often termed flue gas recirculation (FGR) in other combustion systems, such as furnaces. Since CO_2 is a major component of combustion products, it is of fundamental and practical importance to understand how addition of CO_2 to fuel or oxidizer affects flame properties and soot formation. Understanding the effects of CO_2 dilution is also critical in the recently developed oxyfuel combustion technology for reducing CO_2 emissions from large-scale combustion facilities. In oxyfuel combustion the oxidizer is not air but a mixture of high purity oxygen and recycled flue gas to control the flame temperature. With the removal of water vapour the

* Corresponding author.
E-mail address: Fengshan.Liu@nrc-cnrc.gc.ca (F. Liu).

http://dx.doi.org/10.1016/j.combustflame.2015.01.020

combustion products are composed of a very high CO_2 concentration that can be purified to a level suitable for storage.

There have been several studies to investigate the influence of CO_2 dilution effects on soot formation in both counterflow and coflow diffusion flames at atmospheric pressure over the last five decades [3–12]. When a diluent is introduced to either the fuel side or the oxidizer side of a diffusion flame it influences the flame properties and pollutant formation through the following three mechanisms [5]: dilution, thermal, and chemical. The classification and coupling of these three mechanisms were later discussed by Liu et al. [9]. In a very early study of the effect of CO_2 addition McLintock suggested that CO_2 affects soot formation chemically by promoting soot burnout [3]. However, Schug et al. concluded that the effect of CO_2 addition on soot formation suppression is purely thermal [4]. The experimental studies of Du et al. [5] and Gülder and Baksh [7], and to some extent the work of Zhang et al. [6], provided convincing evidence that CO_2 suppresses soot formation not only through dilution and thermal effects, but also through chemical effects. The nature of the chemical effects of CO_2 on soot formation suppression, however, has been subject to debate. Like McLintock [3], Du et al. [5], Zhang et al. [6], and Gülder and Baksh [7] also suggested that the chemical effect of CO_2 is to prompt gas phase soot precursor oxidation by enhancing OH radical concentrations. Based on their experimental measurements of soot volume fraction distributions along the flame centerline of diluted acetylene coflow diffusion flames, Angrill et al. [8] concluded that addition of CO_2 to the oxidizer side reduced soot formation but did not affect soot oxidation close to the visible flame tip. Through numerical modelling of the chemical effects of CO_2 addition to either the fuel or the oxidizer side of a counterflow ethylene/air diffusion flame Liu et al. [9] concluded that CO_2 suppresses soot inception through lowering both temperature and acetylene concentration and enhancing the concentration of OH radical, though soot formation was not included in their numerical calculations. The dominant pathway for the chemical effect of CO_2 was identified to be the reverse reaction of $CO + OH \leftrightarrow CO_2 + H$ [9]. In their experimental studies of the effects of CO_2 addition to the oxidizer side on soot formation in a laminar coflow propane diffusion flame Oh et al. [10,11] found that the chemical effects of CO_2 results in a lower primary particle number concentration in soot inception regions due to reduced flame temperature and increased OH concentration as a result of the reverse reaction of $CO + OH \leftrightarrow CO_2 + H$. In addition, the primary soot particles are smaller. To gain further understanding of the nature of the chemical effects of CO_2 addition on soot formation, Guo and Smallwood conducted a numerical study to investigate how addition of CO_2 to the fuel side influences soot formation in a laminar coflow ethylene/air diffusion flame using detailed chemistry and a sophisticated soot model [12]. The soot model used by Guo and Smallwood was a modified version of Appel et al. [13] to improve the soot concentration prediction in the flame centerline region. Based on their numerical results Guo and Smallwood [12] concluded that the chemical suppression effect of CO_2 addition on soot formation is through reducing soot inception and surface growth rates, but not through enhancing soot oxidation associated with the enhanced OH radical concentrations suggested in earlier studies [3,5–7,9–11]. The findings of Guo and Smallwood are consistent with the experimental measurements of Oh et al. [10,11], who observed reduced soot number density in soot inception regions and smaller primary soot particle diameters. The primary pathway for the chemical effects of CO_2 was again found to be the reverse reaction of $CO + OH \leftrightarrow CO_2 + H$, which reduces the H radical concentrations and consequently pyrene concentrations [12]. As reviewed in [14], H radical activates the radical sites on polycyclic aromatic hydrocarbons (PAH), which is essential for their further growth. It is therefore expected that the reduced H concentration would reduce the role of H-abstraction-C_2H_2-addition (HACA) mechanism in soot inception and soot particle surface growth.

Although most of the experimental and numerical studies conducted so far on the effects of CO_2 addition on soot formation in diffusion flames have reached a consensus that CO_2 suppresses soot formation chemically, in addition to thermal and dilution effects, disagreement exists on how the added CO_2 affects soot formation chemically, i.e., primarily on soot inception, surface growth, or oxidation.

It is also interesting to point out that addition of CO_2 does not always suppress soot formation based on two very recent experimental studies [15,16]. In their experimental study of thermal decomposition of ethylene-CO_2 mixtures at atmospheric pressure, Abián et al. [15] observed an increase in soot production for 25% CO_2 addition, but the tendency of soot formation is decreased for higher CO_2 concentrations. Teini et al. [16] found that a small amount of CO_2 addition can prompt soot formation in very rich $C_2H_2/N_2/O_2/Ar$ mixtures at 10 atm and 1640 K, but otherwise has negligible influence on soot formation in rich $CH_4/N_2/O_2/Ar$ mixtures. Therefore, the chemical effects of CO_2 on soot formation are more complex in premixed mixtures than previously thought.

Many practical combustion devices, such as aircraft gas turbine combustors and diesel engines, operate at elevated pressures to gain higher thermal efficiency and to achieve more compact geometries. Unfortunately, the increased pressure also leads to significantly more production of soot in diffusion flames and the effects of pressure on soot formation processes are still poorly understood due to the complex interplay of physical and chemical processes associated with soot formation in hydrocarbon flames at elevated pressures, though good progress has been made recently in a series of experimental studies of soot formation in laminar coflow diffusion flames at pressures up to 60 atm [17]. Besides the complex nature of soot formation in hydrocarbon diffusion flames, the advance in our understanding of soot formation at elevated pressures is hampered by the challenges of making tractable measurements in sooting flames. These challenges include the enhanced gravity instability, stabilization of tractable laminar diffusion flames, signal trapping, beam steering, and narrowing of the flame at elevated pressures. Despite these difficulties there have been several successful attempts in establishing fairly stable laminar coflow diffusion flames of common gaseous hydrocarbon fuels up to 60 atm as reviewed recently by Karataş and Gülder [17]. The experimental and numerical studies of soot formation in laminar coflow diffusion flames at high pressures conducted so far have provided useful insights into the physical and chemical effects of pressure on the flame structure and soot production [17]. However, only few studies have been conducted so far to investigate the effects of dilution on soot formation at elevated pressures. Berry Yelverton and Roberts investigated the effects of dilution on smoke point through measuring smoke points of diluted methane and ethylene laminar coflow diffusion flames at pressures up to 8 atm [18]. Four diluents were considered, namely helium, argon, nitrogen, and carbon dioxide, to cover a wide range of transport and thermal properties. They observed that at elevated pressures the flame height at the smoke point becomes very insensitive to dilution level and demonstrated the importance of the inlet velocities of the fuel and air streams to the smoke point measurements. In a follow-up study, Berry Yelverton and Roberts reported line-of-sight averaged soot surface temperatures using two-colour soot pyrometry in pure and diluted (with helium, argon, nitrogen, and carbon dioxide) ethylene/air coflow laminar diffusion flames at smoke point and at pressures up to 8 atm [19]. Although Joo and Gülder measured soot temperature and volume fraction distributions in a laminar coflow N_2-diluted ethylene/air diffusion flame in the pressure range of 10 to 35 atm [20], their primary purpose of diluting ethylene with nitrogen was to avoid smoking at pres-

sures up to 35 atm, but not to systematically investigate the effect of dilution on soot formation at high pressures. Several experimental studies of the dilution effects on soot formation at elevated pressures have been conducted very recently [21–25]. Abhinavam Kailasanathan et al. conducted experimental measurements of temperatures and non-fuel hydrocarbon species mole fractions in laminar coflow heavily diluted ethylene/air diffusion flames between 1 and 8 atm [21]. Temperature measurements were limited to 4 atm due to soot deposition on the thermocouple at higher pressures. Four diluents (helium, argon, nitrogen, and carbon dioxide) were investigated in [21] with the dilution ratio being very high at 82% (volume basis). More detailed hydrocarbon and PAH species concentrations in nitrogen-diluted ethylene/air laminar jet diffusion flames at pressure up to 8 atm were reported in [22]. The focus of Refs. [21, 22] was on the dilution effects on soot precursor species concentrations and temperature at elevated pressures, but not directly on soot formation. More recently, Abhinavam Kailasanathan et al. reported line-of-sight averaged soot surface temperature and volume fraction in diluted ethylene/air laminar coflow diffusion flame at pressures up to 8 atm [23]. Again, the four diluents of helium, argon, nitrogen, and carbon dioxide were used for fuel dilution. They observed that the helium diluted flame yields the highest soot surface temperature and volume fraction, while the CO_2-diluted flame yields the lowest soot surface temperature and volume fraction. Although it was concluded in [23] that these low soot concentrations in the diluted flames are not a results of low formation rates, but of enhanced oxidation rates, it was not substantiated, which is at least partially because the experimental results were presented as line-of-sight averages only. In addition, the chemical effects of CO_2 on soot formation suppression at elevated pressures were not isolated or discussed in Refs. [21,23].

Karataş and Gülder [24] and Karataş [25] measured soot temperature and volume fraction distributions in N_2- and CO_2-diluted ethylene/air laminar coflow diffusion flames at two fixed fuel:diluent ratios of 1:2 and 1:3 (mass basis) and at pressures of 5, 10, 15, and 20 atm. By assuming that the difference in the measured soot volume fraction in the N_2- and CO_2-diluted flames can be attributed to the chemical effect of CO_2, Karataş and Gülder [24] and Karataş [25] concluded that the chemical effect of CO_2 on soot production suppression becomes less effective and more complex with increasing pressure based on their experimental results. In particular, their results suggest that soot inception is enhanced and the increase in soot oxidation with CO_2 dilution became less effective on the overall soot yield with increasing pressure.

Although the effects and effectiveness of CO_2 dilution on soot formation in diffusion flames at atmospheric pressure have been conducted in several previous studies discussed earlier, it is not clear if those findings, which are still subject to debate with regard to how CO_2 affects soot formation chemically, are still valid at elevated pressures. The recent experimental study of Karataş and Gülder [24] indeed cast doubt about extending the knowledge of CO_2 effects on soot formation obtained at atmospheric pressure to elevated pressures. The reason for the diminishing chemical effect of CO_2 on soot formation suppression observed by Karataş and Gülder [24] is currently not understood. It is therefore of great importance to investigate the effects of diluents, especially CO_2 for reasons given earlier, on soot formation in diffusion flames at elevated pressures.

In this study soot volume fraction and temperature distributions in laminar coflow N_2-diluted and CO_2-diluted C_2H_4/air diffusion flames at pressures between 5 and 20 atm were experimentally measured using the spectral soot emission (SSE) technique and numerically modelled using two detailed gas-phase C_2 chemistry models and a soot model based on PAH inception and HACA surface growth. CO_2 and N_2 were chosen as diluents due to their abundance and relevance to EGR and oxyfuel combustion technologies. It is of great interest to compare the effect of CO_2 dilution on soot formation with that of N_2 because it has been established that addition of CO_2 to fuel affects soot formation not only through dilution and thermal effects, but also through additional chemical effect at atmospheric pressure [5–7,9,12]. This study was motivated to gain fundamental understanding of the diminishing chemical effect of CO_2 addition on soot formation suppression observed recently by Karataş and Gülder [24]. The objective of this study is to investigate how pressure influences the chemical effects of CO_2 addition to fuel on soot formation in laminar coflow C_2H_4/air diffusion flame over a pressure range of 5 to 20 atm both experimentally and numerically.

2. Experimental method

The high pressure combustion chamber used in this study has been described in detail previously in [20,26–28]. The combustion chamber is designed to sustain pressures up to 110 atm and its internal diameter and height are 24 and 60 cm, respectively. Optical access into the chamber is through three ports mounted at 0°, 90°, and 180° allowing line-of-sight measurements as well as 90° scattering and imaging experiments. A schematic of the experimental setup is shown in Fig. 1.

The burner used in this study is different from that used in previous studies with gaseous fuels [20,26–28]. The basic dimensions of the new annular co-flow burner were based on the design of Miller and Maahs [29] and that provided excellent flame stability in previous studies [20,26–28]. The improved design also allows direct and simultaneous introduction of liquid and gaseous fuels to the burner. An important component of the burner is the fuel nozzle (316L stainless steel) with a sintered metal foam insert (nickel–chromium, RETIMET foam grade 80). The exit diameter of the fuel nozzle is precision machined to 3.0 mm. The inner diameter of the air nozzle is 25.4 mm. A detailed drawing of the burner is shown in Fig. 2.

Ethylene and the diluent (CO_2 and N_2 in this study) were mixed outside the pressure chamber by two calibrated mass flow controllers (Brooks SLA5850) and introduced into the burner from a single port. A constant ethylene mass flow rate of 0.48 mg/s was

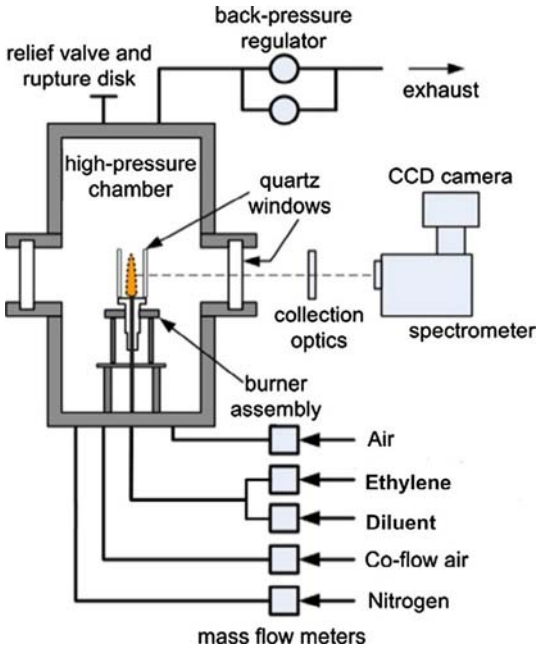

Fig. 1. Schematic of the experimental setup.

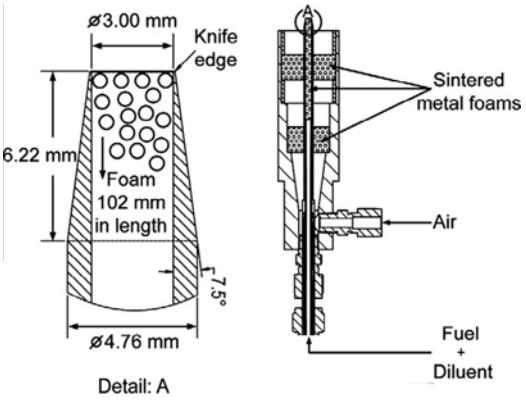

Fig. 2. Details of the fuel burner.

maintained throughout this study. This mass flow rate corresponds to a carbon flow rate of 0.41 mg/s, which matches the carbon flow rate of previous experiments [26–28]. The co-flow air flow rate was maintained at 0.34 g/s for all experiments. Both fuel and air were delivered to the burner at room temperature. The dilution rate (fuel:diluent) of 1:2 by mass was studied for each diluent. This dilution rate was chosen to avoid emitting soot from the tip of the flames at pressures up to 20 atm. Additional considerations in this choice of dilution ratio are as follows. The fuel was diluted in such a way that the mass fraction of the diluent was matched. This is justified based on the study of Axelbaum and Law who explained in [30] that the residence time in a buoyancy-dominated laminar co-flow diffusion flame, such as in the flames investigated in this study, is proportional to QS, here Q is the fuel mixture flow rate (volumetric basis) and S the stoichiometric ratio (mass basis). Further, it has been shown that the flame diameter scales with $(QS)^{0.25}$ [31], meaning that residence times in a flame do not change if QS remains constant. It was further argued that QS calculated from only the reactant part of a fuel/inert mixture is sufficient [30]. It should also be noted that the laminar flame height scales inversely with molecular diffusivity or directly with molecular weight [19]. Since the dilution levels considered in this study are not very high, the effect of molecular diffusivity on flame height should be quite small, though the CO_2-diluted flame tends to be slightly higher based on such consideration. Therefore, the flame height and diameter can be considered only dependent on the fuel flow rate, and dilution with an inert does not significantly affect the flame shape. Since the fuel flow rate was maintained constant in this study, flame properties at equal heights in different flames can be directly compared because the residence times can be considered the same. However, it is recognized that it is also possible to conduct the experiments by keeping the same fuel:diluent volume ratio, which should also maintain the flame shape. Keeping the same fuel:diluent mass ratio may result in different dilution effect from keeping the same volume ratio, but it is not possible to completely separate the chemical effect of CO_2 from its thermal and dilution effects experimentally, recalling that the objective of comparing the experimental results of N_2 dilution with those of CO_2 dilution is to identify the chemical effect of CO_2. This issue will be addressed in numerical modelling and discussed through comparison between experimental and numerical results.

Soot temperature and volume fraction distributions were measured using the spectral soot emission (SSE) technique. The theory and experimental setup of the SSE technique were described in detail in several previous studies [20,26,27,32,33]. In SSE, line-of-sight radiation emission from soot is measured along chords through the flame in the visible spectrum. A series of emission projections at a given height in the flame can be inverted to obtain radially resolved emission rates from which temperature and soot volume fraction can be determined when soot optical properties are known [32,33]. The emitted radiation from soot first passes through an adjustable aperture and lens unit. For the current study an aperture diameter of about 6.2 mm and associated f-number of f/48 was used. The lens selected for this study is an achromatic doublet lens with a focal length of 300 mm. The lens has an anti-reflective coating, effective within the wavelength range of 650–1050 nm. The purpose of the lens is to image the flame radiation onto the entrance slit of the spectrometer. The lens is positioned to produce a 1:1 image. The entrance to the spectrometer contains two slits; the vertical slit is approximately 25 μm in width, and the horizontal slit is approximately 290 μm in height. The slit sizes play a role in the resulting spatial resolution of the collected data [32].

The spectrometer is an imaging Czerny-Turner spectrometer that internally uses aspheric mirrors. The spectrometer grating used for this task has a blaze wavelength of 775 nm and is manufactured with 300 groves/mm. The spectrometer has a dispersion of approximately 18.84 nm/mm. Soot emission is measured over a wavelength range of 690–945 nm. The total array size of the CCD is 1340 × 400 pixels. However, due to the restricted size of the entrance slit, a region of interest of size 1340 × 80 pixels was selected. Combined with the previously mentioned spectrometer and grating, the CCD camera is capable of capturing an approximate wavelength spread of 505 nm across the camera array, providing a spectral step size of 0.377 nm/pixel. Knife-edge scans across a diffuse light source located at the object plane indicated a horizontal spatial resolution of 70 μm over the depth of field defined by the burner nozzle exit diameter. The vertical spatial resolution was inferred to be approximately 290 μm. To calibrate the spectral axis of the CCD array, a pencil style neon calibration lamp was used. The system is calibrated for radiation intensity using a filament lamp, with a calibration traceable to NIST, placed inside the chamber.

The uncertainty in the SSE soot temperature and volume fraction has been previously discussed in [26,28,32,34]. Two main sources of SSE soot temperature uncertainty are the wavelength dependence of soot absorption function $E(m)$ over the spectral range of detection, namely 690–945 nm, and attenuation of emission by soot present between the emission location and the detector or self-absorption. The sensitivity study of Snelling et al. showed that a change in slope from a constant $E(m)$ to a linear variation of $E(m)_\lambda$ increasing at a rate of 40%/μm leads to a 50 K increase in the measured temperature, meaning about 3% on a measured temperature of 1700 K and a 30% decrease in the estimated soot concentration [32]. A recent systematic analysis of the effect of self-absorption of soot emission found that neglect of self-absorption can cause underestimation of soot temperatures in the peak soot concentration regions by about 60 K under conditions similar to the present study, but the influence is small to the soot volume fraction [35]. The overall uncertainty in the SSE soot temperature measurements can be estimated to be about 5.5% (95% confidence level). The uncertainty in the measured soot temperature is dominated by the uncertainty in the wavelength dependence of $E(m)$ and neglect of emission attenuation in the data analysis. The uncertainty in the SSE soot volume fraction is estimated to be 40% (again 95% confidence level), which is primarily attributed to uncertainty in the soot temperature measurements.

3. Numerical model and computational details

The governing equations for mass, momentum, energy, species are solved in a fully coupled fashion. The details of the governing equations and solution methods have been described in several previous studies [36–38]. A sectional method is used to describe

the soot particle dynamics, leading to resolution of additional transport equations for sectional soot aggregate and primary particle number densities [36,37]. The conservation equations are solved in axisymmetric cylindrical coordinates using a finite volume method. The stiffness of the equation system associated with the use of detailed gas-phase chemistry and the sectional soot model was handled by solving the species and soot number density transport equations in a fully coupled way [36,37]. Since the resultant system of equations is highly non-linear and very computationally demanding, parallel computation is necessary with the help of a domain decomposition method [37]. Radiative heat transfer by radiating species (CO, CO_2, H_2O, and soot) is accounted for by solving the radiative transfer equation using the discrete ordinate method coupled to a statistical narrow-band correlated-K (SNBCK) based wide-band model [39].

The fixed sectional soot model used in this study has been employed and described in several previous studies [36,37,40]. The range of soot aggregate mass is divided into a number of discrete sections, each with a prescribed representative mass. The evolution of each section is governed by two transport equations for the number densities of soot aggregate and primary particles. The incipient soot particles are assumed to be spherical and belong to the first section. As in previous studies [36–38], 35 sections were used in the sectional model with a spacing factor of 2.35. Further details of the sectional soot model are available in [36,37].

The soot kinetics model is largely based on the work of Appel et al. [13]. Although soot inception is likely to be the result of collisions among various large PAHs, for simplicity soot inception is assumed to be the result of collision of two pyrene molecules (A_4), following the work of Appel et al. [13]. Surface growth and oxidation are assumed to follow the HACA mechanism by using the same parameters as in [13], except the steric factor α, which is described below. Soot surface growth due to PAH condensation is also taken into account as collisions of A_4 molecules with soot aggregate surface. The condensation rate is calculated by the collision theory between A_4 molecules and aggregates [40]. Based on the consideration that not all collisions lead to successful condensation, a PAH condensation efficiency is introduced and assumed to be 0.5 [37].

Two gas-phase reaction mechanisms were employed in the present numerical modelling. One is the C_2 chemistry of Appel et al. [13], which contains 101 species and reactions for formation of PAHs up to pyrene (A_4). This reaction mechanism, along with its PAH formation reactions, has been shown to predict soot volume fraction distributions reasonably well in the flame wings of laminar coflow ethylene/air diffusion flames at atmospheric pressure [36], where soot formation is dominated by HACA surface reactions. In addition, the C_2 chemistry of Appel et al. [13] has also been found to be capable of capturing the synergistic effect of dimethyl ether addition to fuel on PAH and soot formation in a laminar coflow ethylene/air diffusion flame at atmospheric pressure [38]. A recent study by Dworkin et al. [41], however, has shown that the Appel et al. C_2 mechanism underpredicts concentrations of PAHs in a laminar coflow C_2H_4/air diffusion flame at atmospheric pressure, especially along the flame centerline region. The other gas-phase reaction mechanism employed in the present study is the C_2 reaction mechanism of Slavinskaya and Frank [42], which consists of 94 species and PAHs also up to A_4 and was shown to perform better in soot formation modelling along the flame centerline in a laminar coflow C_2H_4/air diffusion flame at atmospheric pressure [41].

When the Appel et al. mechanism [13] (hereafter ABF) was used, the steric factor α was set to $\alpha = 0.004\exp(10800/T)$ subject to the restriction of $0 \leqslant \alpha \leqslant 1$. As pointed out in [43] the value of α given by this expression is essentially unity at temperatures below 1950 K, i.e., almost everywhere in soot formation regions in most diffusion flames. When the Slavinskaya and Frank mechanism [42] (hereafter DLR) was used, a constant α of 0.078 was used based on two recent studies of soot formation in laminar coflow ethylene diffusion flames at atmospheric pressure [41,43].

Numerical calculations were conducted for laminar coflow N_2- and CO_2-diluted C_2H_4/air flames at 5, 10, 15, and 20 atm by using the same burner geometry and inlet conditions as those in the experiments described above. Numerical calculations were performed over a computational domain of 1.79 cm (z) × 0.81 cm (r) with 210 (z) × 88 (r) control volumes. A non-uniform mesh was used with a resolution of 0.05 mm in the r-direction and 0.066 mm in the z-direction near the burner exit. In the case of nitrogen dilution the inlet ethylene mole fraction is $X_{C2H4} = 0.333$ and mean inlet fuel stream velocity is $U_F = 17.91/p$ cm/s (p is in atm), while in the case of carbon dioxide dilution the inlet ethylene mole fraction is $X_{C2H4} = 0.44$ and the mean inlet velocity of the fuel stream is $U_F = 13.57/p$ cm/s (p is in atm). A nearly uniform inlet velocity profile was assumed to the fuel stream and a uniform profile was assumed to the air stream. The inlet air stream velocity is assigned as $U_A = 57.82/p$ cm/s (p is in atm). The inlet temperatures of the fuel and air stream are assumed to be 300 K in all calculations. All the calculations were carried out using 16 CPUs. Iterations were stopped when the relative change in the maximum soot volume fraction remained below 1×10^{-4} for more than 200 iterations.

To directly illustrate the variation of the chemical effect of CO_2 on soot formation with pressure additional calculations were performed with FCO_2 dilution, following the methodology used successfully in previous studies [9,12]. Here FCO_2 is a fictitious species that possesses identical thermal and transport properties and the third body collision efficiency as CO_2 but is excluded from chemical reactions. In addition, FCO_2 is also considered as a radiating species to participate in radiative heat transfer and has the same radiative properties as CO_2. Numerical calculations were performed for N_2, CO_2, and FCO_2 dilution using the ABF mechanism, but only for CO_2 and FCO_2 dilution using the DLR mechanism. Table 1 provides a summary of the different cases of fuel stream dilution investigated in the numerical modelling.

Among the cases given in Table 1 that were numerically modelled, Cases ABF-1, ABF-3, and DLR-1 directly simulated the experiments of N_2 and CO_2 dilution for a fixed fuel:diluent mass ration of 1:2. Case ABF-2 was included to evaluate if there are any different dilution effects between N_2 and CO_2 dilution at a fixed fuel:diluent mass ratio, i.e., between Cases ABF-1 and ABF-3. Case ABF-2 has the same dilution ratio as Case ABF-3 on mole or volume basis. As such, Cases ABF-2 and ABF-3 have the same fuel stream inlet velocity, which is about 32% lower than that in Case ABF-1 (13.57 vs. 17.91 cm/s at 1 atm). As mentioned above, Cases ABF-4 and DLR-2 were considered to completely isolate the chemical effects of CO_2, which are illustrated by the differences in numerical results between Cases ABF-3 and ABF-4, as well as between Cases DLR-1

Table 1
Different cases of fuel stream dilution investigated numerically.

Case	Diluent	Fuel:diluent mass ratio	Fuel stream compositions (mole fraction)
ABF mechanism			
1	N_2	1:2	$X_{C2H4} = 0.333$, $X_{N2} = 0.667$
2	N_2	1:1.27	$X_{C2H4} = 0.44$, $X_{N2} = 0.56$
3	CO_2	1:2	$X_{C2H4} = 0.44$, $X_{CO2} = 0.56$
4	FCO_2	1:2	$X_{C2H4} = 0.44$, $X_{FCO2} = 0.56$
DLR mechanism			
1	CO_2	1:2	$X_{C2H4} = 0.44$, $X_{CO2} = 0.56$
2	FCO_2	1:2	$X_{C2H4} = 0.44$, $X_{FCO2} = 0.56$

and DLR-2. All the cases shown in Table 1 were calculated at pressures 5, 10, 15, and 20 atm. In the following discussion the N_2-diluted flame refers to the case of a fuel:diluent ratio of 1:2 on mass basis unless otherwise explicitly indicated.

4. Results and discussion

4.1. Visible flame appearance

The visible flame appearances of N_2- and CO_2-diluted ethylene/air diffusion flames at pressure from 1 to 20 atm are shown in Fig. 3 as still flame photography. The flame shape is strongly affected by pressure. The pressure effect on the flame shape of laminar coflow diffusion flames has been extensively discussed in the literature [17,20,26,44] and therefore it will not be repeated here. At atmospheric pressure, the luminous zone only appears at the flame tip due to dilution by nitrogen or carbon dioxide. Dilution by either nitrogen or carbon dioxide at a 1:2 ratio is very effective to reduce the flame sooting tendency so that the flames remain non-smoking even at 20 atm. It is noted that without dilution the ethylene/air diffusion flame becomes smoking at 9 atm. It is evident from Fig. 3 that the CO_2-diluted flames produce less soot at lower pressures based on the size of the luminous zone. When the pressure is increased to 5 atm, the blue flame zone is limited to a small region just above the burner rim. At higher pressures, the blue zone is no longer visible and the visible flame region expands towards the fuel nozzle. The visible flame height does not change significantly for $p \geqslant 5$ atm. The visible flame height of the N_2-diluted flame is consistently slightly higher than that of the CO_2-diluted one at pressures between 1 and 20 atm. At 20 atm, the visible flame heights for the N_2- and CO_2-diluted flame are around 9 mm and 8.5 mm, respectively. In addition, at 20 atm soot wings start to become clearly visible for both the N_2- and CO_2-diluted flames, implying that the smoke point condition is almost reached.

In the present experiments the fuel mass flow rate is fixed and the flame is buoyancy-dominated, the flame height is nearly independent of pressure as shown in Fig. 3. Moreover, flame properties at equal heights in different flames (or at different pressures) can be directly compared because the variation of residence time with the vertical distance from the burner exit is the same, with the exception in a small region just above the burner exit.

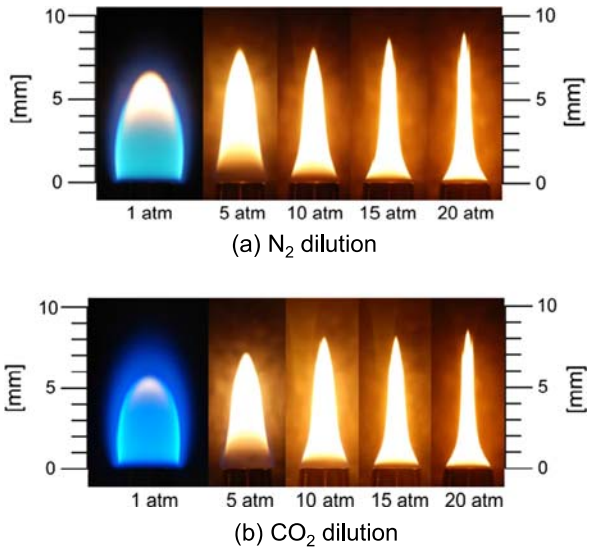

Fig. 3. Flame photography of the N_2- and CO_2-diluted ethylene/air diffusion flames from 1 to 20 atm.

4.2. Effect of pressure on temperature and soot volume fraction

The measured and calculated two-dimensional distributions of temperature and soot volume fraction in the CO_2-diluted flames at 5, 10, 15, and 20 atm are displayed in Figs. 4–6. Results for the N_2-diluted flames are qualitatively similar to those shown in Figs. 4–6. It is noted that SSE can only measure soot temperature in regions where soot is present. The measured temperature distributions indicate that the flame temperatures at pressures between 5 and 20 atm vary between 1400 and 1900 K. At 5 atm, the temperatures are around 1800 K with relatively small variations within the flame. As the pressure increases, temperatures in all flames decrease and temperature variation within a flame increases. At higher pressures, temperatures are relatively lower at the lower half of the flame, and they increase towards the flame tip, presumably due to energy released from soot and PAH oxidation reactions at the upper half of the flame. The drop in the flame temperature with increasing pressure is due to the increased radiative losses from soot particles, and the increase in the temperature variation throughout the flame is likely due to increased soot volume fraction gradients observed at higher pressures. While the enhanced radiation heat loss due to higher soot loadings with increasing the pressure is clearly responsible for the lowered temperatures, variation in the pathways of fuel decomposition and oxidation with pressure could also play a role in flame temperature as revealed in the significant decrease in the mole fraction of O, H, and OH radicals with increasing pressure presented later. Figure 4 shows that soot loading in the flame is significantly increased with increasing pressure. Two other observations can be made from Fig. 4. First, the peak soot volume fraction occurs in the flame centerline region at 5 atm. At higher pressures ($\geqslant$10 atm), however, the peak soot volume fraction appears in the annular region, i.e., the flame wings, which may be an indication in the change of relative importance of soot surface growth by HACA and soot surface condensation to soot loading with increasing pressure. Second, soot starts to appear earlier (closer to the burner rim) as the pressure increases, which is due to enhanced fuel pyrolysis (and therefore soot inception) associated with air entrainment into the flame base [44,45].

Figures 5 and 6 display the calculated soot temperature and volume fraction distributions using the ABF and DLR mechanisms, respectively, between 5 and 20 atm. The peak flame temperatures appear in the annular region low in the flame and decrease with increasing pressure with a higher rate at lower pressure. For example, the peak temperature drops about 22 K (2004.1–1981.7 K) when the pressure increases from 5 to 10 atm. However, it only decreases by 3 K (1964.5–1961.5 K) as the pressure increases from 15 to 20 atm. Although the peak flame temperatures decrease only modestly with increasing pressure, temperatures in the upper portion of the flame centerline region (between about 6–10 mm) decrease significantly, which is in qualitative agreement with the SSE results shown in Fig. 4. As discussed above, the decrease in temperature in the upper portion of the flame is attributed to radiative heat loss from soot. The visible flame heights are well captured by the ABF mechanism at all four pressures. At 5 atm, the predicted flame height is somewhat shorter than those at higher pressures, in agreement with the experimental observations shown in Fig. 3. The predicted peak soot volume fractions also increase significantly with increasing pressure. It is interesting to point out that at 20 atm a strip of soot pierces through the flame tip, but is still fully oxidized at an axial location of about 10.5 mm, Fig. 5(d). This feature is again in qualitative agreement with the flame photo shown in Fig. 3(b). Although the soot model coupled with the ABF mechanism is able to reproduce the main features of the pressure effect on soot formation observed experimentally, its main drawback lies in the very low predicted

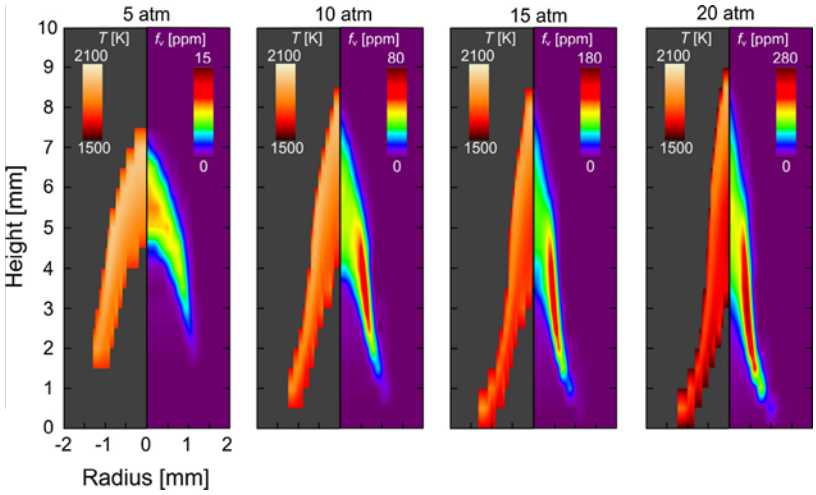

Fig. 4. Measured distributions of radially resolved soot volume fraction and temperature measurements in CO_2-diluted-ethylene/air (1:2 by mass) laminar diffusion flames from 5 atm to 20 atm.

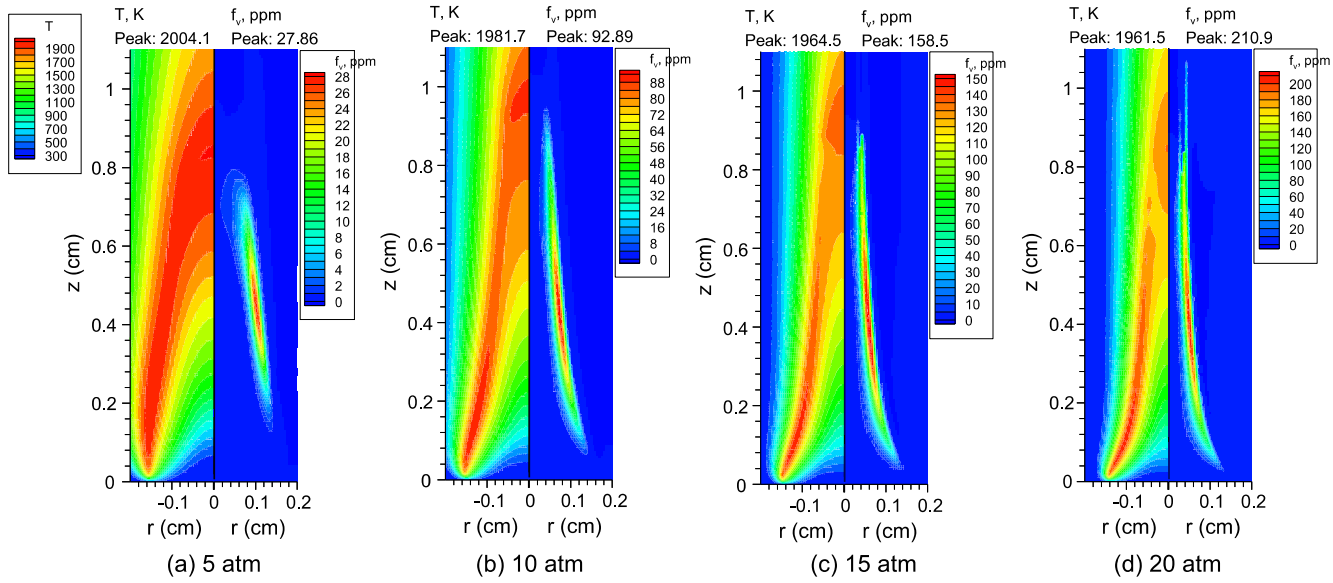

Fig. 5. Calculated distributions of soot temperature and volume fraction using the ABF mechanism in CO_2-diluted-ethylene/air laminar diffusion flames from 5 to 20 atm.

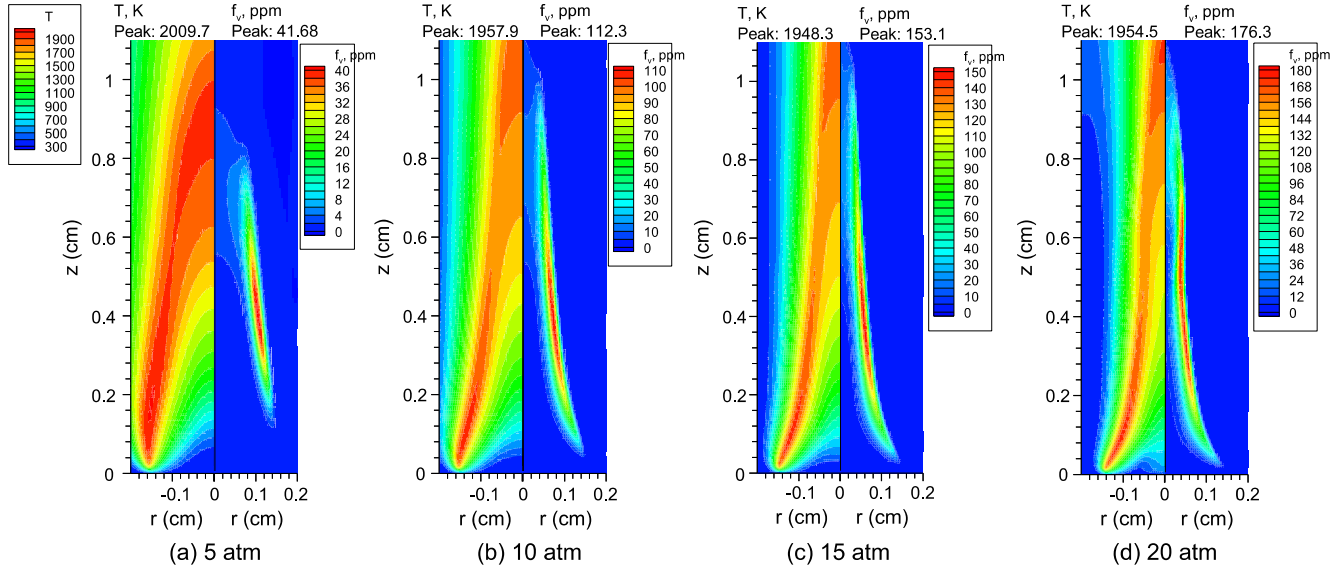

Fig. 6. Calculated distributions of soot temperature and volume fraction using the DLR mechanism in CO_2-diluted-ethylene/air laminar diffusion flames from 5 to 20 atm.

soot concentrations in flame centerline region compared to the experimental results shown in Fig. 4. Another main discrepancy between the prediction and experiment is the soot volume fraction distribution at 5 atm, where the measured peak value occurs in the centerline region, Fig. 4, but the model prediction is in the annular region, Fig. 5(a). At higher pressures, the predicted peak soot volume fractions also occur at the flame wings, in agreement with the experimental results.

The temperature distributions predicted by the DLR mechanism shown in Fig. 6 are overall similar to those by the ABF mechanism displayed in Fig. 5. However, the peak temperatures in the DLR results decrease more rapidly with increasing pressure. The predicted soot loading also increases fairly rapidly as the pressure increases. The improvement in the predicted soot concentration in the flame centerline regions by the DLR mechanism is visible, but not remarkable. Moreover, the DLR mechanism overpredicts the visible flame heights at all the four pressures by about 2 mm. Similar to the results of the ABF mechanism at 5 atm, the predicted soot peak also occurs in the annular region, instead of in the flame centerline. The visible soot strip at 20 atm observed in the flame photo, Fig. 3(b), and in the ABF prediction, Fig. 5(d), however, did not appear in the DLR results.

Although discrepancies between the measured and calculated temperature and soot volume fraction distributions exist, especially the near absence of soot in the flame centerline regions in the ABF results due to the missing of some PAH formation pathways in the Appel et al. mechanism [13] and the overprediction of visible flame height in the DLR results, the model correctly captures the overall influence of pressure on temperature and soot volume fraction, i.e., temperatures decrease while soot volume fractions increase significantly with increasing pressure.

While it is recognized that the peak soot volume fraction could occur at different flame heights when the pressure increases, it is still very useful to compare the peak soot volume fraction at different pressures, since the peak soot volume fraction can be used as a measure of how the flame sooting tendency varies with pressure. Such comparison has been made previously in the literature, e.g., [26,44,46]. The measured and calculated peak soot volume fractions are compared in Fig. 7. At 5 atm, both the measured and the calculated (ABF mech.) peak soot volume fractions in the CO_2-diluted flame are lower than those in the N_2-diluted flame. At higher pressures of 10 and 15 atm, the difference in the peak soot volume fraction in the two flames decreases. At 20 atm, however, both the measured and the calculated (ABF mech.) peak soot volume fractions in the CO_2-diluted flame are actually slightly higher. This trend suggests that CO_2 is more effective than N_2 in soot formation suppression at lower pressures but the effectiveness of CO_2 diminishes with increasing pressure. This point will be discussed further later. Although both the measured and calculated maximum soot volume fractions increase rapidly with pressure, the model overpredicts the peak soot volume fractions at 5 and 10 atm, but underpredicts them at 20 atm in both the N_2- and CO_2-diluted flames, especially when the DLR mechanism is used. It is evident from Fig. 7 that the measured peak soot volume fraction exhibits a faster increase rate with pressure than the predicted one by either the ABF or the DLR mechanism. The pressure exponents n for the measured and calculated maximum soot volume fraction, i.e., $f_{v,max} \propto p^n$, in the pressure ranges of 5–10 atm and 10–20 atm are summarized in Table 2.

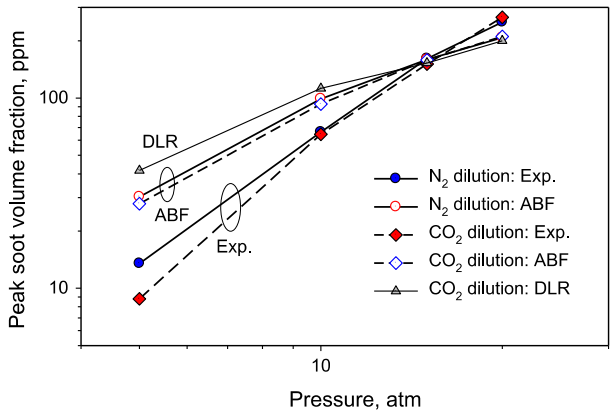

Fig. 7. Variation of the measured and calculated peak soot volume fraction with pressure.

As expected, the measured peak soot volume fraction in the CO_2-diluted flame has the largest pressure exponent between 5 and 10 atm, which is related to the higher effectiveness of CO_2 dilution on soot suppression at lower pressures. At the higher pressure range of 10 to 20 atm, the pressure exponents in the CO_2- and N_2-diluted flames are similar. The DLR mechanism predicted the weakest pressure dependence of the peak soot volume fraction in the entire pressure range considered.

To assess the sensitivity of the sooting propensity of fuel to pressure the soot yield has often been used [20,25,26,28,45]. It represents the percentage of carbon in the fuel converted to soot and is defined as $\eta_s = \dot{m}_s/\dot{m}_c$, where $\dot{m}_c$ is the carbon mass flow rate at the nozzle exit (here 0.41 mg/s) and $\dot{m}_s$ is the mass flow rate of carbon, in the form of soot at a given flame height, and is calculated using the following expression

$$\dot{m}_s(z) = 2\pi\rho_s \int v_z(r,z) f_v(r,z) r dr \quad (1)$$

where v_z is the axial velocity, $\rho_s = 1.8$ g/cm^3 is the soot density, f_v is the soot volume fraction, r is the radial coordinate, and z is the axial height. The measured and calculated maximum soot yields using the ABF mechanism are compared in Fig. 8. In the evaluation of soot yield based on measured soot volume fraction, the axial velocity was estimated using the relationship $v_z(z) = \sqrt{2az}$, where a is an acceleration constant estimated as 32 m/s^2 based on numerical simulations [45]. The measured soot yield indicates that the soot yield increases continuously in a nearly linear fashion in both the N_2- and CO_2-diluted flames over the pressure range of 5–20 atm. The N_2-diluted flame has a higher carbon yield than the CO_2-diluted one and the differences remain similar between 5 and 20 atm, implying that CO_2 is still more effective than N_2 in suppressing soot formation at elevated pressures. The calculated soot yields are higher at 5 and 10 atm but substantially lower at 20 atm than the measured ones in both the N_2- and CO_2-diluted flames, consistent with the observations made from Fig. 7 for the peak soot volume fractions. In fact, the calculated soot yields increase only slightly when the pressure is increased from 15 to 20 atm, though the peak soot volume fraction still increases significantly as shown in Fig. 7. The slight increase in the calculated soot yields between 15 and 20 atm indicates the balance of the two competing factors between flame narrowing and higher soot volume fractions. The reason for the continuous increase in the

Table 2
The pressure exponents of the peak soot volume fraction.

	5–10 atm	10–20 atm
Exp.: CO_2 dilution	2.87	2.05
Exp.: N_2 dilution	2.29	1.94
ABF: CO_2 dilution	1.74	1.19
ABF: N_2 dilution	1.71	1.08
DLR: CO_2 dilution	1.43	0.83

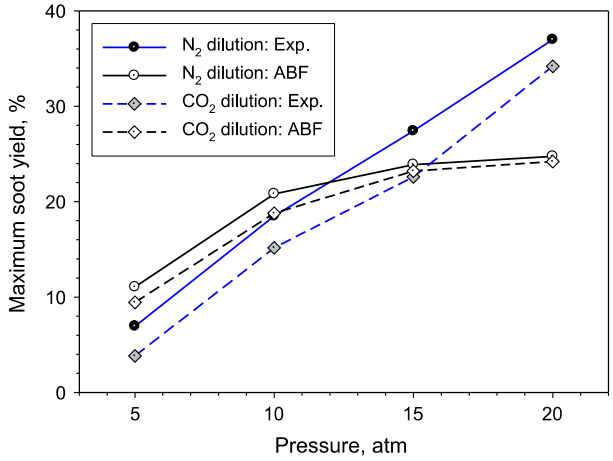

Fig. 8. Comparison of the measured and calculated maximum soot yields at pressures between 5 and 20 atm in the N_2- and CO_2-diluted flames.

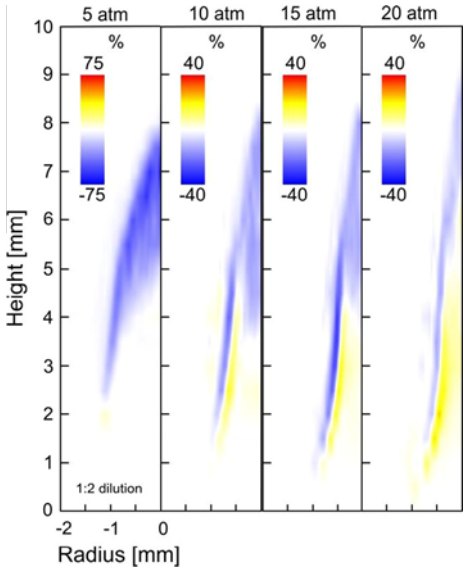

Fig. 9. The percentage change in soot volume fraction between the CO_2- and N_2-diluted flames from the experiments.

measured soot yields between 10 and 20 atm is due to the larger increase in the peak soot volume fractions than the calculated ones shown in Fig. 7. Comparison between Figs. 7 and 8 indicates that soot yield is a better way to assess the sooting ability of a flame since it takes into account of both flame shape (through integration across the flame radially) and soot loading. In particular, at 20 atm the peak soot volume fraction in the N_2-diluted flame is slightly lower but it still has a higher soot yield. The reason for these reverse trends is likely related to the slightly larger radius in the N_2-diluted flame.

4.3. The chemical effect of CO_2

Both the experimental and modelling results indicate that CO_2 is still more effective than N_2 in suppressing soot formation at a fixed fuel:dilutent mass ratio (note that more N_2 is added to fuel on volume basis) between 5 and 20 atm, consistent with the findings of previous studies at atmospheric pressure [4,5,7] and recent studies at elevated pressures [18,23]. The better soot formation suppression ability of CO_2 is due to its thermal effect (higher specific heat) and additional chemical effects [5,7,9,24,25]. However, it is not clear how pressure affects the chemical effect of CO_2 on soot formation suppression. By arguing that the specific heats of CO_2 and N_2 are similar (they differ by less than about 8%) and the temperature distributions in the N_2- and CO_2-diluted flames are also quite similar, Karataş ascribed most of the difference in soot volume fraction between the N_2- and CO_2-diluted flames (at a constant fuel:diluent ratio on mass basis) to the chemical effects of CO_2 [25]. To illustrate and quantify the chemical effect of CO_2 on soot formation suppression, Karataş [25] defined the following quantity

$$\Delta f = \frac{f_{v,CO_2} - f_{v,N_2}}{(f_{v,N_2})_{max}} \times 100\% \qquad (2)$$

to represent the fractional change in local soot volume fraction due to the chemical effect of CO_2. In Eq. (2), $(f_{v,N2})_{max}$ is the maximum soot volume fraction at the pressure under consideration. Results of Δf based on the measured soot volume fractions at the four pressures are shown in Fig. 9. By definition of Δf given in Eq. (2), negative values mean the soot volume fractions in the CO_2-diluted flame are lower or vice versa. At 5 atm, Δf is negative throughout the flame, so that soot volume fractions in the CO_2-diluted flames are consistently lower. At higher pressures, Δf is negative in the upper portion of the flame and in the outer edge of the flame wings; however, positive values of Δf start to emerge in the inner edge of the flame wings low in the flame starting at 10 atm. Karataş [25] interpreted the positive values of Δf as enhancement of soot inception by CO_2 addition, since the locations of positive values apparently coincide with fuel decomposition and soot inception regions. Figure 9 also shows that the magnitude of negative values decrease and the positive values increase with increasing pressure, implying that the chemical effects of CO_2 dilution on soot inception enhancement and overall soot formation suppression become increasingly more significant and less significant, respectively, as the pressure is increased. If the assumption of Karataş [25] is valid, i.e., the difference in soot volume fraction between the N_2- and CO_2-diluted flames is largely due to the chemical effects of CO_2, his interpretation of the experimental results shown in Fig. 9 seems plausible. However, the question is if his assumption is valid. The answer to this question cannot be found from experimental investigation since it is not possible to conduct experiments in which the thermal and dilution effects of CO_2 can be completely separately from its chemical effects. Instead, the answer has to be sought by performing detailed numerical calculations for CO_2- and FCO_2-dilution, since the differences in the numerical results between the cases of CO_2- and FCO_2-dilution can be unambiguously attributed to the chemical effects of CO_2 [9,12].

Since the numerical results reproduce the main features of experimental measurements of the effects of pressure on the flame structure and soot loading over the pressure range considered, it is reasonable to state that the numerical model is capable of identifying the various effects of dilution as the difference between different cases discussed below. Before presenting the numerical counterparts to the experimental results shown in Fig. 9, it is useful to examine the calculated peak soot volume fractions first. As mentioned earlier, the peak soot volume fraction is a useful quantity to illustrate the pressure and dilution effects on soot formation. The calculated peak soot volume fractions are compared in Table 3. For the purpose of providing a direct comparison between the experimental and numerical results, the measured peak soot volume fractions are also included in Table 3. It is noted that the measured peak soot volume fractions and some calculated ones, including Cases ABF-1, ABF-3, and DLR-1, are shown in Fig. 7.

It is first observed from Table 3 that the DLR mechanism predicted almost the same peak soot volume fractions at pressures

up to 15 atm, regardless of CO_2 or FCO_2 dilution, suggesting that this mechanism fails to capture the chemical effects of CO_2 on soot formation. For this reason, numerical results calculated by the DLR mechanism will not be further considered in the following discussion. The reason for the failure of the DLR mechanism to predict the chemical effects of CO_2 is unclear and such investigation is beyond the scope of this study. On the other hand, the ABF mechanism predicted lower peak soot volume fractions in the case of CO_2 dilution than those in FCO_2 dilution, i.e., it captures the chemical effects of CO_2 on soot formation suppression that has been shown experimentally and numerically in previous studies conducted at atmospheric pressure [5,7,9,12]. It is interesting to point out that the predicted peak soot volume fractions in Cases ABF-1 and ABF-3 correctly represent the trend of the relative magnitude of these two cases observed in the measured values. For example, the predicted peak soot volume fraction in the N_2-diluted flame, Case ABF-1, is higher at 5, 10, and 15 atm, but lower at 20 atm than that in the CO_2-diluted flame, Case ABF-3. The same trend can also be observed in the measured values.

Two other observations can also be made from Table 3. First, Cases ABF-1 (N_2-dilution) and ABF-4 (FCO_2-dilution, without chemical effects) have different peak soot volume fractions with those in Case ABF-4 being higher, even they have the same fuel:diluent mass ratio, implying that the N_2-diluted flame in the experiments of Karataş and Gülder [24] cannot truly represent the inert counterpart of the CO_2-diluted flame. In addition, the fact that the peak soot volume fractions in Case ABF-1 are lower than those in Case ABF-4 suggests that N_2 dilution with the same fuel:diluent ratio on mass basis as in CO_2 (and FCO_2) dilution does introduce additional dilution effects due to its higher dilution on mole basis. Secondly, Case ABF-2 has higher peak soot volume fractions than Case ABF-4, which is mainly due to the thermal effect of FCO_2 dilution relative to N_2 dilution at the same dilution ratio on mole basis, since the difference in the transport properties between N_2 and CO_2 is quite small. Nevertheless, neither N_2 dilution matching the fuel:diluent ratio on mass basis nor N_2 dilution matching the fuel:diluent ratio on mole basis to CO_2 dilution can be used to completely isolate the chemical effects of CO_2 dilution on soot formation suppression. This conclusion is substantiated by the fact that the peak soot volume fraction of Case ABF-4 falls between Cases ABF-1 and ABF-2 at all four pressures.

The above discussion suggests that the assumption of Karataş and Gülder [24] to ascribe the difference in soot volume fraction between the N_2- and CO_2-diluted flames to the chemical effects of CO_2 is questionable. This point is illustrated through the fractional change in the local soot volume fraction between Cases ABF-1 and ABF-3 and between Cases ABF-1 and ABF-4. The local soot volume fraction between Cases ABF-1 and ABF-3 is first examined. Using Eq. (2) and the predicted soot volume distributions in Cases ABF-1 and ABF-3 the distributions of fractional change in local soot volume fraction at the four pressures are shown in Fig. 10. Although the magnitude of fractional change in the numerical results deviates from the measured one, the distributions are qualitatively similar at pressures between 5 and 20 atm. It is remarkable to observe that the numerical results capture the higher soot volume fractions in the inner edge of the flame rings low in the flame in the CO_2-diluted flame at pressures above 10 atm shown in Fig. 9, though at 10 atm such observation is not clearly visible in Fig. 10(b). Based on the above discussion of the results given in Table 3, the higher soot volume fractions in the inner edge of the flame wings low in the CO_2-diluted flame is likely caused by the additional dilution effect of N_2 at a fixed fuel:diluent mass ratio and should not be explained as enhancement of soot inception by CO_2 addition. Under the experimental conditions of Karataş and Gülder [24] the mole fraction of ethylene in the fuel stream is 0.333 in the N_2-diluted flame and 0.44 in the CO_2-diluted flame, respectively, as shown in Table 1. In other words, there is more N_2 added to the fuel than CO_2 on volume basis, which is likely responsible for the lower soot volume fractions low in the flame in the N_2-diluted flame than in the CO_2-diluted one at pressures above 10 atm, Figs. 9 and 10, rather than the enhancement of soot inception by the chemical effects of CO_2 suggested by Karataş [25]. To verify this conjecture the fractional changes in the local soot volume fraction between the CO_2- (Case ABF-3) and FCO_2-diluted (Case ABF-4) flames are compared in Fig. 11. In this case, quantities associated with N_2-dilution in Eq. (2) are replaced by those with FCO_2-dilution. The results in Fig. 11 remain consistently negative throughout the flame at all four pressures, meaning that the chemical effects of CO_2 always suppress soot formation during inception low in the flame, and surface growth and oxidation processes in the higher portion of the flames.

It is useful to examine the temperature distributions in the CO_2- and FCO_2-diluted flames due to the importance of temperature to soot formation, even though any difference in temperature between the two flames is still a consequence of the chemical effect of CO_2. The temperature distributions in the CO_2-diluted flame at pressures between 5 and 20 atm are very close to those in the FCO_2-diluted flame, with the latter being only slightly higher. The difference in the peak temperature decreases from about 8 K at 5 atm to about 3 K at 20 atm. Therefore, such a small difference in temperature is not responsible for the observed difference in the soot loading between the CO_2- and FCO_2-diluted flames and the chemical effect of CO_2 on temperature can be considered negligible.

The additional dilution effect in the N_2-diluted flame is believed to be responsible for its slightly taller visible flame height than the CO_2-diluted flame at all pressures studied shown in Fig. 3 [47]. As a result of a slightly taller visible flame height of the N_2-diluted flame, the fractional change in the local soot volume from Eq. (2) should always be negative near the tip of the N_2-diluted flame. Although results shown in Fig. 11 confirm that the positive values of fractional change in the local soot volume fraction between the N_2- and CO_2-diluted flames is due to the additional dilution effect of N_2 associated with the higher N_2 mole fraction in the fuel stream, they do not explain why the positive values low in the flame occur only at pressures above 10 atm, but not at 5 atm, Figs. 9 and 10. The answer to this question lies in the relative importance of the additional dilution effect of N_2 and the chemical effect of CO_2 to soot inception suppression. The additional dilution effect in the N_2-diluted flame causes a slight delay in the formation of large hydrocarbons and PAHs [47], and therefore soot inception. On the other hand, soot inception in the CO_2-diluted flame is also further supressed by the CO_2 chemical effects (in addition to the dilution effect). Therefore, it is not obvious if soot inception starts earlier in the N_2-diluted or in the CO_2-diluted flame, which

Table 3
The peak soot volume fractions calculated by the ABF and DLR mechanisms.

Case	Diluent	5 atm	10 atm	15 atm	20 atm
Predicted $f_{v,max}$ (ppm) by ABF mechanism					
1	N_2	30.28	99.02	159.3	208.2
2[a]	N_2	36.11	119.9	189.4	241.8
3	CO_2	27.86	92.89	158.3	210.9
4	FCO_2	34.79	104.7	169.7	222.1
Predicted $f_{v,max}$ (ppm) by DLR mechanism					
1	CO_2	41.69	112.3	153.1	186.1
2	FCO_2	41.38	112.1	153.2	192.3
Measured $f_{v,max}$ (ppm)					
1	N_2	13.5	66.2	161.0	251.0
2	CO_2	8.8	64.4	151.0	266.0

[a] Case 2 has a different dilution ratio from Case 1. See Table 1 for details.

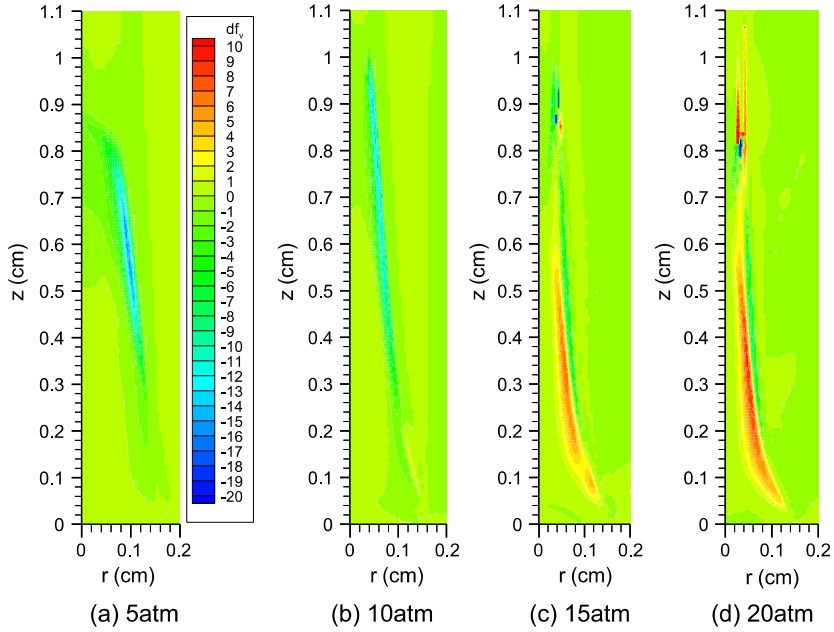

Fig. 10. The percentage change in soot volume fraction between the CO_2- and N_2-diluted flames from the numerical calculations using the ABF mechanism.

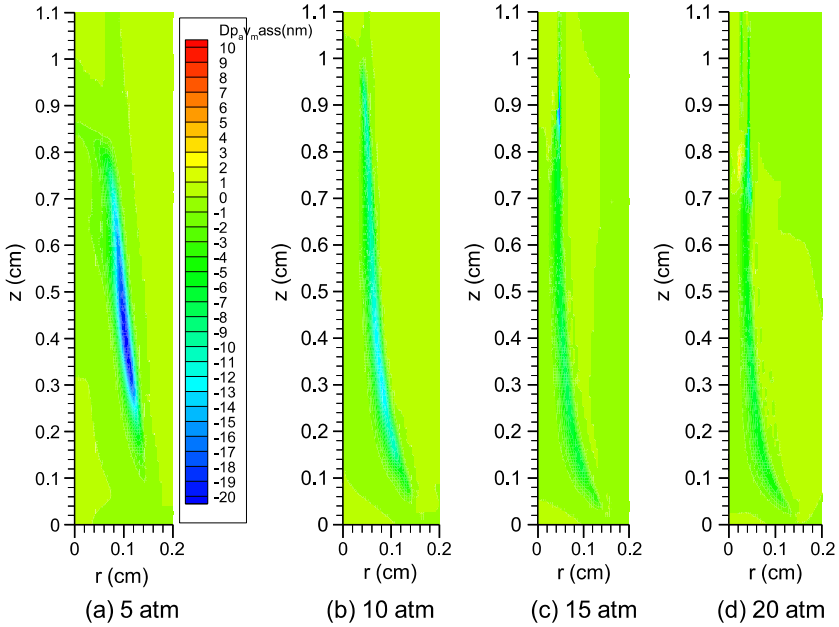

Fig. 11. The percentage change in soot volume fraction between the CO_2- and FCO_2-diluted flames from the numerical calculations using the ABF mechanism.

depends on the relative importance of the additional dilution effect of N_2 (in the N_2-diluted flame) and the chemical effect of CO_2 (in the CO_2-diluted flame) on soot inception suppression. Before discussing further on this subject, the pressure dependence of the chemical effects of CO_2 is examined first.

4.4. Influence of pressure on the chemical effects of CO_2

Both the numerical results of the ABF mechanism and the experimental results presented in Section 4.3 clearly indicate that CO_2 plays a chemical role in soot formation suppression in the pressure range considered, as identified from the difference in the results of Cases ABF-3 (CO_2 dilution) and ABF-4 (FCO_2 dilution) shown in Table 3 and Fig. 10 and the difference in the experimental results between N_2- and CO_2-diluted flames, though the latter is contaminated by the additional N_2 dilution effect. However, the pressure dependence of such chemical effects has not been analyzed. The percentage reduction of the calculated peak soot volume fraction by the chemical effect of CO_2 is shown in Fig. 12, which is calculated as

$$\eta = \frac{f_{v\,max,FCO_2} - f_{v\,max,CO_2}}{f_{v\,max,FCO_2}} \times 100\% \quad (3)$$

where $f_{vmax,FCO2}$ and $f_{vmax,CO2}$ represent the calculated peak soot volume fractions in the FCO_2- and CO_2-diluted flame, respectively. It is evident that the percentage reduction in the peak soot volume

fraction decreases continuously and the rate of reduction also decreases significantly with increasing pressure. Although the soot volume fraction distribution in the N_2-diluted flame cannot adequately represent that in the FCO_2-diluted flame, especially at higher pressure of 15 and 20 atm, the percentage decrease in the measured peak soot volume fractions in the CO_2- diluted flame from those in the N_2-diluted flame also exhibit a rapid decrease when the pressure is increased from 5 to 10 atm (not shown). To further illustrate the pressure dependence of the chemical effect of CO_2 on soot formation suppression, the total soot loadings in the FCO_2- and CO_2-diluted flames are calculated and the chemical effect of CO_2 on the percentage reduction in the total soot loading is compared. The total soot loading in a flame is calculated using the following expression

$$\Phi = \int_0^{h_f} \int_0^{r_f(z)} f_v 2\pi r dr dz \tag{4}$$

where h_f and $r_f(z)$ are the visible flame height and visible flame radius, respectively. Results of the total soot loadings and the percentage reduction in total soot loading by the chemical effect of CO_2 are also plotted in Fig. 12. The percentage reduction in the total soot loading is calculated in the same way as that for the peak soot volume fraction, i.e., using Eq. (3) with f_{vmax} replaced by Φ. As expected from the numerical results shown earlier, the total soot loadings in both flames increase rapidly with increasing pressure and the rate of increase continues to drop as the pressure is increased. The percentage reduction in the total soot loading by the chemical effect of CO_2 also continuously decreases with increasing pressure, displaying an overall similar trend as that of the peak soot volume fraction. A similar analysis of the maximum soot yields shown in Fig. 8 also indicates that the percentage reduction in the maximum soot yield by the chemical effects of CO_2 also decreases with increasing pressure, again supporting the notion that the chemical effect of CO_2 on soot formation suppression diminishes with increasing pressure. It is noted that in the analysis of the experimental data shown in Fig. 8 the results in the N_2-diluted flame were considered as equivalent to those in the FCO_2-diluted one. On the other hand, the additional dilution effect of N_2 is not expected to depend on pressure. Indeed, the peak soot volume fractions in Case ABF-1 are about 16% lower than those in Case ABF-2 at all four pressures. It should be pointed out that the difference in soot volume fraction between Cases ABF-1 and ABF-2 is caused by the additional dilution effect of N_2.

The pressure dependence of the fractional change in the local soot volume fraction between the CO_2- and N_2-diluted flames shown in Figs. 9 and 10 can be explained by the diminishing chemical effects of CO_2 on soot formation suppression. At lower pressures, such as 5 atm, the chemical effect of CO_2 on soot inception and surface growth suppression in the CO_2-diluted flame outweighs the additional dilution effect in the N_2-diluted flame. As a result, soot volume fractions in the CO_2-diluted flame are lower than those in the N_2-diluted one everywhere and the fractional change in the local soot volume fraction is negative throughout the flame. At higher pressures, however, the chemical effects of CO_2 on soot formation suppression decrease while the additional dilution of N_2 remains unchanged. As such, soot inception takes place earlier (at a lower distance to the burner exit surface) and at higher rates low in the CO_2-diluted flame when the pressure is sufficiently high, which occurs at 10 atm in the experiments and at 15 atm in the modelling as shown inn Figs. 9 and 10, respectively. This is why the soot volume fractions are higher in the inner edge of the flame wings in the CO_2-diluted flame and the fractional change in the local soot volume fraction in the inner edge of the flame wings low in the flame becomes positive at higher pressures (15 and 20 atm) in Figs. 9 and 10. To demonstrate the earlier and larger soot inception rates in the CO_2-diluted flame than in the N_2-diluted flame the distributions of soot inception rate in these two flames (Cases ABF-1 and ABF-3) at 15 atm are compared in Fig. 13. It is evident that soot inception occurs slightly earlier and at higher rates in the CO_2-diluted flame low in the flame, except in a small region where the soot inception rates in the N_2-diluted flame are higher, Fig. 13(b). The earlier and larger soot inception in the CO_2-diluted flame leads to earlier and higher soot surface growth rates by C_2H_2 addition low in the flame. Figure 14 shows the distributions of soot surface growth rates by C_2H_2 addition in the CO_2- and N_2-diluted flames and their difference at 15 atm. It is evident that the soot surface growth rates by C_2H_2 addition in the CO_2-diluted flame are significantly higher than those in the N_2-diluted flame low in the flame and in the inner edge of the flame wings, except in a very small area. The earlier and higher soot inception and surface growth eventually leads to higher soot volume fractions in the CO_2-diluted flame in the inner edge of the flame wings shown in Figs. 9 and 10.

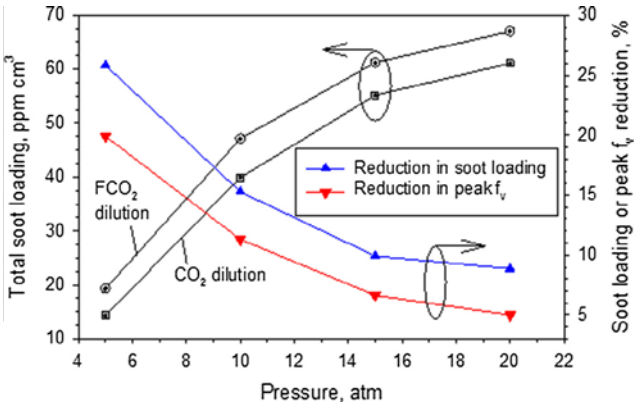

Fig. 12. Variation of the calculated total soot loadings in the CO_2- and FCO_2-diuted flames and the percentage reduction in the total soot loading and the peak soot volume fraction between the two flames with pressure.

4.5. How pressure influences the chemical effects of CO_2 on soot formation suppression

The above discussion has established that CO_2 suppresses soot formation chemically at elevated pressures and the relative contribution of chemical effects of CO_2 to soot formation reduction decreases with increasing pressure. It is of importance to understand how pressure influences the CO_2 chemical effects on soot formation suppression.

Pressure affects flame and soot formation both physically and chemically. The physical effects of pressure consist of its influence on mixture density ($\rho \propto p$) and binary diffusion coefficient ($D_{ij} \propto p^{-1}$). The chemical effect of pressure on diffusion flame and soot formation has received little attention, though such effect has been recognized by Liu et al. [44] and more recently discussed by Mandatori and Gülder [48]. The chemical effect of pressure on soot formation has been demonstrated in a recent numerical study of Guo et al. [49], who showed that the relative importance of benzene forming reactions to benzene and the contributions of inception, HACA, and PAH condensation to soot loading varies as the pressure increases from 1 to 8 atm in a laminar coflow undiluted C_2H_4/air diffusion flame.

Increasing pressure increases the mixture density proportionally, leading to much higher gas-phase reaction rates as well as inception, surface growth (HACA), surface condensation rates for soot formation. On the other hand, increasing pressure also prompts three-body recombination reactions, which suppress the formation of important radicals (namely O, H, and OH) in the system, and hence potentially alters the relative importance of various reactions to PAH formation and soot inception and surface growth

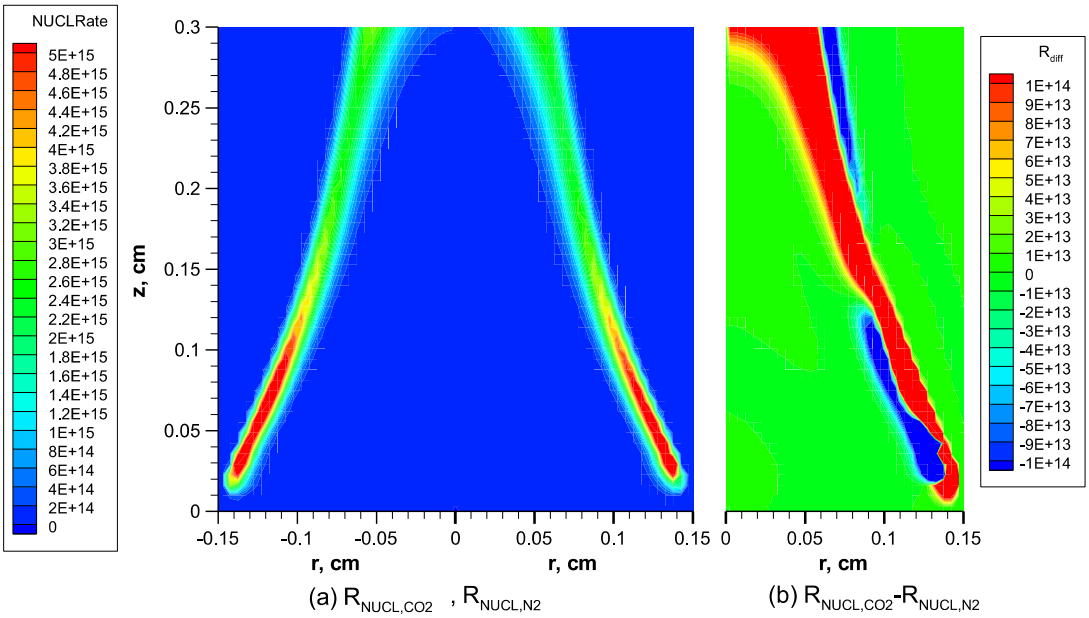

Fig. 13. Distributions of soot inception rate (in #/cm^3 s) in the CO_2- and N_2-diluted flames, (a), and their difference, (b), at 15 atm.

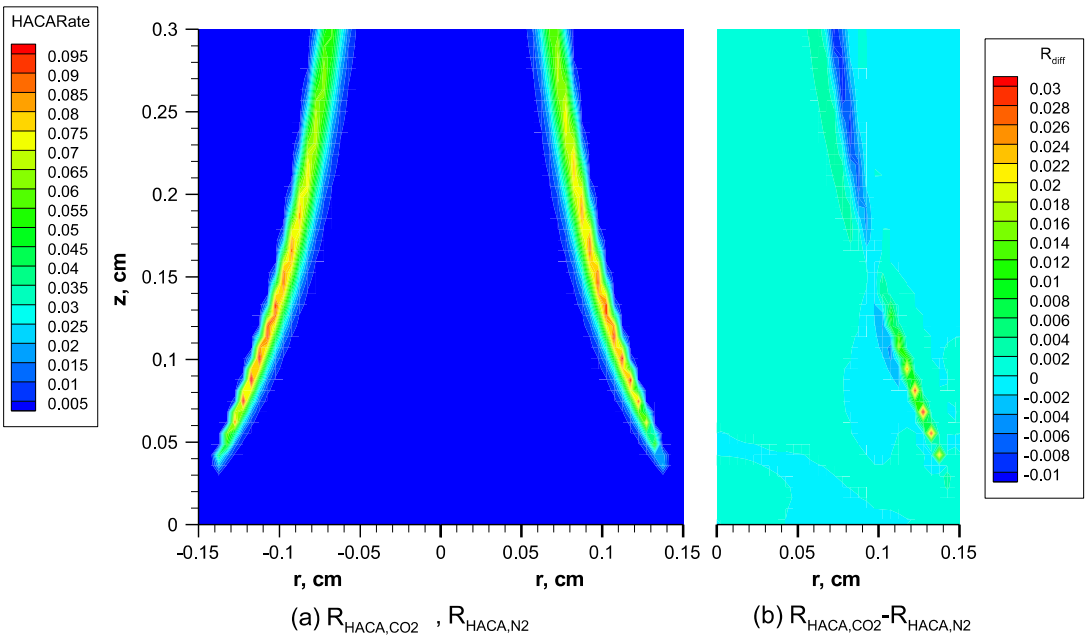

Fig. 14. Distributions of soot surface growth rate by C_2H_2 addition (in g/cm^3 s) in the CO_2- and N_2-diluted flames, (a), and their difference, (b), at 15 atm.

processes [44,49]. It is therefore expected that pressure can significantly influence the chemical effect of CO_2 on the flame structure (temperature and species concentrations) and soot production, since at elevated pressures the mole fractions of the most important radicals in combustion (O, H, and OH) can be substantially lowered through enhanced three-body recombination reactions. The reduced radical concentrations of O, H, and OH in turn can alter the relative importance of pathways for fuel decomposition and oxidation and hence the flame temperature and structure in general. The focus here is on the chemical effects of CO_2 on soot formation.

The calculated peak O, H, and OH mole fractions in the N_2-, CO_2-, and FCO_2-diluted C_2H_4/air flames are summarized in Table 4. An examination of the distributions of these radicals shows that the maximum values are always at locations just above the burner rim. It is evident from Table 4 that the maximum mole fractions of all the three radicals decrease significantly with increasing pressure, especially O and H radicals. For example, in the N_2-diluted flame when the pressure increases from 5 to 20 atm the maximum mole fraction of O and H radicals decreases by a factor of about 7 and 5.8, respectively, while the maximum value of OH radical decreases only by a factor of 2.3. A decrease in the mole fraction of a species with increasing pressure signifies that pressure suppresses this species chemically. A similar decrease in the mole fractions of O, H, and OH radicals with increasing pressure can also be observed in the FCO_2-diluted flame. In the CO_2-diluted flame, how-

Table 4
Calculated maximum mole fractions of O, H, and OH in N_2-, CO_2, and FCO_2-diluted ethylene flames. Ratio denotes the ratio of mole fraction at 5 atm over that at 20 atm.

Flame	Max. mole fraction	Pressure (atm)				Ratio
		5	10	15	20	
N_2-diluted	O	1.113E−3	4.131E−4	2.318E−4	1.597E−4	6.97
	H	1.459E−3	7.019E−4	4.163E−4	2.535E−4	5.76
	OH	3.073E−3	2.098E−3	1.589E−3	1.316E−3	2.34
CO_2-diluted	O	1.069E−3	3.923E−4	2.217E−4	1.506E−4	7.10
	H	1.323E−3	6.068E−4	3.477E−4	2.585E−4	5.18
	OH	3.01E−3	2.099E−3	1.592E−3	1.312E−3	2.29
FCO_2-diluted	O	1.123E−3	4.157E−4	2.328E−4	1.563E−4	7.18
	H	1.497E−3	6.852E−4	4.024E−4	3.047E−4	4.91
	OH	3.170E−3	2.181E−3	1.648E−3	1.347E−3	2.35

Table 5
Calculated peak mole fractions of C_2H_2, A_1, and A_4 in the CO_2- and FCO_2-diluted ethylene flames at 5–20 atm.

	5 atm	10 atm	15 atm	20 atm
CO_2-diluted flame				
C_2H_2	2.614E−2	2.146E−2	1.809E−2	1.637E−2
A_1	2.432E−4	3.383E−4	4.069E−4	4.726E−4
A_4	1.448E−7	1.361E−7	1.243E−7	1.225E−7
FCO_2-diluted flame				
C_2H_2	2.757E−2	2.182E−2	1.835E−2	1.656E−2
A_1	2.673E−4	3.592E−4	4.298E−2	4.977E−4
A_4	1.563E−7	1.389E−7	1.262E−7	1.237E−7

Table 6
Percentage reduction in the peak mole fractions of C_2H_2, A_1, and A_4 by the chemical effect of CO_2 in the CO_2-diluted ethylene flame.

	5 atm	10 atm	15 atm	20 atm
C_2H_2	5.19	1.65	1.42	1.15
A_1	9.01	5.83	5.33	5.05
A_4	7.32	2.02	1.56	0.94

ever, a further reduction in the mole fraction of these three radicals, relative to those in the FCO_2-diluted flame, can be observed, which is attributed to the chemical effect of CO_2.

The decrease in O, H, and OH mole fractions with increasing pressure can have significant influences on soot formation through altering the mole fractions of soot precursor or inception (pryene) and surface growth (acetylene) species and their direct participation in the HACA sequences. According to the HACA sequences for PAH and soot growth, H radical plays an important role [13,14].

Examination of the reaction rates in reactions involving CO_2 in the present numerical results reveals that the primary pathway for the chemical effect of CO_2 is still the reverse reaction of $CO + OH \leftrightarrow CO_2 + H$ (R30), identified in previous studies conducted at atmospheric pressure [9,12]. The reverse reaction of R30 becomes relatively less effective with increasing pressure, simply because of the significant decrease in the mole fraction of H radical shown in Table 4.

As the first ring structured species in the ethylene flame, formation of benzene is critical for the subsequent formation of PAHs. Besides benzene, acetylene and pyrene are also of great importance in soot surface growth through the HACA mechanism and in soot inception modelled by collision of two pyrene molecules. The calculated peak mole fractions of acetylene, benzene, and pryene in the CO_2- and FCO_2-diluted flames are compared in Table 5. Although the peak concentrations of all these three species occur in the flame centerline region, rather than in the annular region low in the flame where soot inception first takes place, the peak

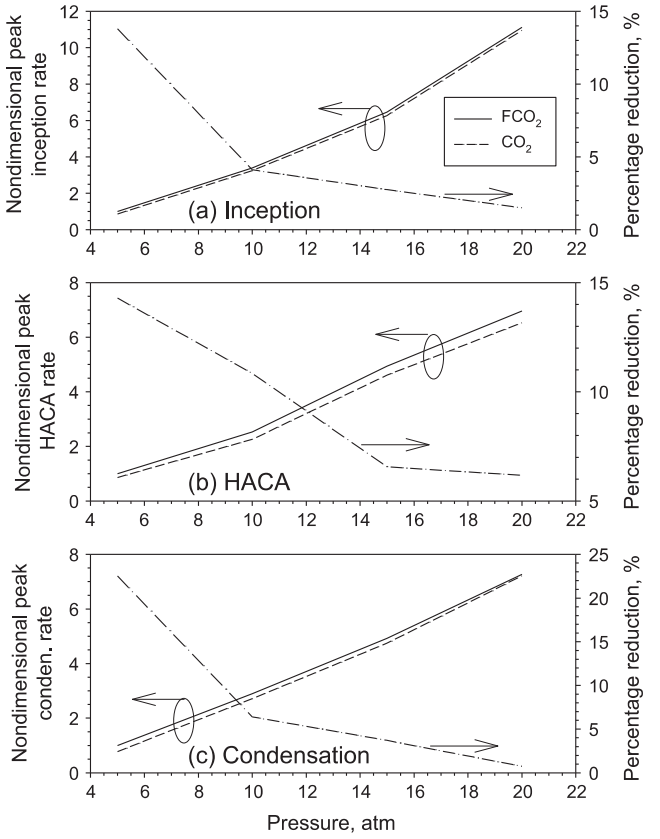

Fig. 15. Variation of the nondimensional peak soot formation rates and the percentage reduction of these rates by the chemical effect of CO_2 with pressure.

mole fractions can be conveniently used as a good surrogate to evaluate the influence of pressure and the chemical effect of CO_2 on the concentrations of these species. Table 5 indicates that the peak mole fractions of C_2H_2 and A_4 decrease and the peak mole fraction of A_1 increases with increasing pressure in both the CO_2- and FCO_2-diluted flames. It is noted that the peak mole fractions of C_2H_2 and A_4 shown in Table 5 are the values with their consumption to form soot accounted for. Such coupling has a relatively small influence on the C_2H_2 concentrations, but has a very large impact on the A_4 concentrations [49]. The decrease and increase of the peak C_2H_2 and A_1 mole fractions with increasing pressure, respectively, are consistent with the experimental measurements of Abhinavam Kailasanathan et al. [21,22].

The differences in the peak mole fractions between the CO_2- and FCO_2-diluted flames are due to the chemical effect of CO_2. It

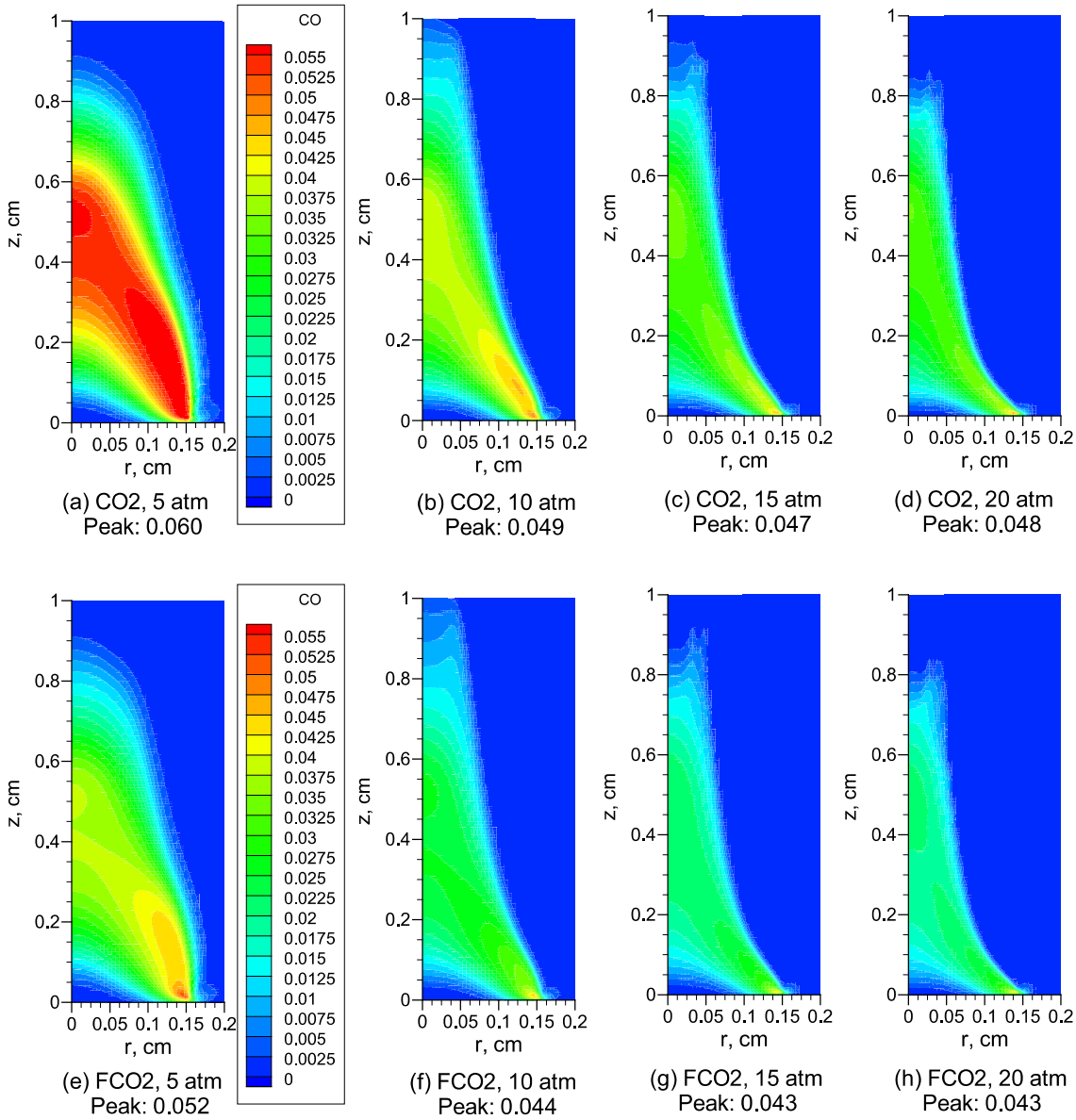

Fig. 16. Distributions of CO mole fraction predicted by the ABF mechanism for CO_2 dilution, (a)–(d), and for FCO_2 dilution, (e)–(h), at the four pressures investigated.

is evident from Table 5 that the chemical effect of CO_2 leads to lower peak mole fractions of all these three species at 5–20 atm investigated. To illustrate how the chemical effect of CO_2 on the peak mole fractions of these species varies with pressure, the percentage changes in the peak mole fractions of these species are given in Table 6, where the percentage changes are calculated using Eq. (3) by replacing the peak soot volume with the peak mole fraction. Similar to the results shown in Fig. 12 for the peak soot volume fraction and the total soot loading, the chemical effect of CO_2 on the peak mole fractions of C_2H_2, A_1, and A_4 also diminishes monotonically with increasing pressure. Given the roles played by C_2H_2 and A_4 in soot formation, it is straightforward to expect that the chemical effect of CO_2 becomes less significant with increasing pressure, as shown earlier in the experimental and numerical results.

Although it can be expected from the results shown in Tables 5 and 6 that the chemical effect of CO_2 on all the three soot formation steps, namely inception, surface growth by C_2H_2 addition (HACA), and surface growth by PAH condensation, are weakened with increasing pressure, the rates of the three soot formation steps are nevertheless analyzed. Figure 15 displays the nondimensional peak soot formation rates in the CO_2- and FCO_2-diluted flames. Nondimensionalization was made by the respective peak rate in the FCO_2-diuted flame at 5 atm. Figure 15 shows that the rates of all the three soot formation steps increase significantly with increasing pressure with the inception rate increases the fastest and the increases in the rates of HACA and PAH condensation are similar. These results are in contrast to the findings of Guo et al. [49] who showed in a undiluted ethylene/air diffusion flame between 1 and 8 atm that the local peak PAH condensation rate increases the fastest with increasing pressure while the C_2H_2 addition rate increases with pressure at a much slower rate than the inception and PAH condensation rates. The rates of all three soot formation steps in the CO_2-diluted flame are lower than those in the FCO_2-diluted one, as a result of the chemical effect of CO_2. Also plotted in Fig. 15 are the percentage reduction in the three rates

evaluated again using Eq. (3) with the peak soot volume fraction replaced by the respective soot formation rates. These results indicate that the chemical effect of CO_2 on the rates of all the three soot formation steps weakens with increasing pressure, with the effect on the PAH condensation rate decreases fastest and the effect on the HACA rate decreases the slowest. In addition, the chemical effect of CO_2 on soot formation suppression weakens very rapidly when pressure increases from 5 to 10 atm, but the weakening becomes very gradual with further increase in pressure.

The results presented in Table 5 and Fig. 15 suggest that the chemical effect of CO_2 on soot formation suppression is to reduce the mole fractions of C_2H_2 and A_4 and the rates of all three soot formation steps, but not by prompting soot oxidation. This conclusion is consistent with the numerical study of Guo et al. conducted at atmospheric pressure [12].

It is important to point out that the chemical effect of pressure, the chemical effect of CO_2, and PAH and soot formation processes are strongly coupled through H radical. The chemical effect of pressure lowers H radical mole fraction by enhancing three-body recombination reactions. The added CO_2 affects the flame and PAH and soot formation chemically through competing for H radical via the reverse reaction of $CO + OH \leftrightarrow CO_2 + H$. While H radical strongly affects PAH and soot surface growth through the hydrogen abstraction step in HACA sequences, which in turn affects the rates of soot inception and the subsequent surface growth. Although the chemical participation of CO_2 through the reverse reaction of $CO + OH \leftrightarrow CO_2 + H$ consumes H radical, it also promotes the OH radical, which is efficient in oxidizing soot and soot precursors. On the other hand, the reduced H radical concentration also weakens the chain branching reaction $H + O_2 \leftrightarrow O + OH$ to produce O and OH radicals in regions of the reaction zone where the concentrations of both H and O_2 are appreciable. On the fuel rich side of the reaction zone where the O_2 concentrations are very low, however, it is expected that the production of OH due to the chemical effect of CO_2 is more significant due to the absence of competition for H by O_2 through $H + O_2 \leftrightarrow O + OH$. Consequently, it is likely that the chemical effect of CO_2 also lowers soot production through enhanced OH oxidation. An examination of the OH distribution at 5 atm shows that the OH concentrations are indeed slightly higher on the fuel side of the reaction zone in the CO_2 diluted flame than those in the FCO_2 diluted one low in the flame between about 0.5 cm < z < 2.5 cm; however, the opposite is observed on the air side of the reaction zone. Nevertheless, the chemical effect of CO_2 primarily reduces the H radical concentration, but only weakly affects the OH radical concentration. These points can also be observed in the results shown in Table 4 and are consistent with the finding of Guo and Smallwood [12].

The calculated distributions of CO mole fraction in the CO_2- and FCO_2-diluted flames using the ABF mechanism are compared in Fig. 16 with the peak value indicated in each plot. The four plots on the top row are for the CO_2 dilution case at 5, 10, 15, and 20 atm. The bottom four plots are for the FCO_2 dilution case at the corresponding pressures. In both the CO_2 and FCO_2 diluted flame the CO mole fractions decrease with increasing pressure. The CO mole fractions are significantly higher in the CO_2-diluted flame than those in the FCO_2-diluted flame, to compare the plots in the top row to those at the bottom row. The significantly higher CO mole fractions in the CO_2 diluted flame are consistent with the pathway of the CO_2 chemical effect: the reverse reaction of $CO + OH = CO_2 + H$. It is seen that he difference in the CO mole fraction between the two flames becomes smaller with increasing pressure, which is consistent with the notion that the chemical effect of CO_2 decreases with increasing pressure. Finally, it is interesting to point out that the distributions of CO mole fraction predicted by the DLR mechanism in both the CO_2 and FCO_2 flame at different pressures are very similar to those shown in Fig. 16. This is a good indication that the DLR mechanism captured the chemical effect of CO_2 through the reverse reaction of $CO + OH = CO_2 + H$. The nearly absence of the chemical effect of CO_2 in terms of soot formation in the results of the DLR mechanism deserves further investigation.

5. Conclusions

Experimental measurements and numerical calculations were conducted in laminar coflow nitrogen- and carbon dioxide-diluted ethylene/air diffusion flames at pressure between 5 and 20 atm to investigate if and how pressure influences the effectiveness of the chemical effect of CO_2 in the suppression of soot formation. The fuel flow rate was maintained constant in all the experiments and numerical calculations. The diluent of either nitrogen or carbon dioxide was added to the fuel stream at a fixed fuel:diluent ratio of 1:2 on mass basis. The numerical results obtained using the ABF mechanism reproduce the main features of the experimental results and observations. The DLR mechanism failed to capture the chemical effect of CO_2 and predicted significantly taller visible flame heights than the experimental observations. The following conclusions can be drawn based on the experimental and numerical results:

1. Soot loading increases rapidly with increasing pressure in both the nitrogen- and carbon dioxide-diluted flames. The model predicts weaker pressure dependence of the peak soot volume fraction and soot yield than the measurements.
2. Carbon dioxide is still more effective than nitrogen to suppress soot formation at elevated pressures up to 20 atm under the present conditions mainly due to its additional chemical effect.
3. The primary pathway for the chemical effect of CO_2 at elevated pressures is still its competition for H radical to form CO and OH, i.e., $CO_2 + H \rightarrow CO + OH$, identified in previous studies conducted at atmospheric pressure.
4. There is an additional dilution effect in the nitrogen-diluted flame at a fixed fuel:diluent ratio on mass basis. The soot volume fractions in the nitrogen-diluted flame can only be used to approximately represent those in the "non-reactive CO_2"-diluted flame to qualitatively identify the chemical effect of CO_2. The chemical effect of CO_2 may not be completely isolated by experiments.
5. The chemical effect of CO_2 lowers the concentrations of the critical soot formation species, including H, C_2H_2, benzene, and pyrene, as well as the rates of all three soot formation processes, i.e., inception, surface growth through C_2H_2 addition, and surface growth through pyrene condensation. The chemical effect of CO_2 on soot loading reduction is primarily through reducing the rates of soot formation steps, rather than prompting soot oxidation.
6. The relative effectiveness of the CO_2 chemical effect on soot formation suppression was found to decrease with increasing pressure from both measurements and numerical results.
7. The diminishing chemical effect of CO_2 is caused by the significant decrease in the H radical mole fraction as pressure increases, as a result of the enhanced three-body recombination reactions to reduce radical concentrations. The reduced H radical mole fraction weakens the chemical role of CO_2 in the system.

Acknowledgments

Operational funds for the work performed at the University of Toronto have been provided by Natural Sciences and Engineering

Research Council Canada through Discovery and Strategic Project grants. Mingyan Gu thanks the National Natural Science Foundation of China (Grant Nos. 51306001 and 51376008) for financial support.

References

[1] M.Z. Jacobson, Nature 409 (2006) 695–697.
[2] I.M. Kennedy, Proc. Comb. Inst. 31 (2007) 2757–2770.
[3] I.S. McLintock, Combust. Flame 12 (1962) 217.
[4] K.P. Schug, Y. Manheimer-Timnat, P. Yaccarino, I. Glassman, Combust. Sci. Technol. 22 (1980) 235–250.
[5] D.X. Du, R.L. Axelbaum, C.K. Law, Proc. Combust. Inst. 23 (1990) 1501–1507.
[6] C. Zhang, A. Atreya, K. Lee, Proc. Combust. Inst. 24 (1992) 1049–1057.
[7] Ö.L. Gülder, M.F. Baksh, Influence of carbon dioxide dilution on soot formation in diffusive combustion, The Combustion Institute Canadian Section 1993 Sprint Technical Meeting, May 9–12, 1993, Université Laval, Quebec, Canada.
[8] O. Angrill, H. Geitlinger, T. Streibel, R. Suntz, H. Bockhorn, Proc. Combust. Inst. 28 (2000) 2643–2649.
[9] F. Liu, H. Guo, G.J. Smallwood, Ö.L. Gülder, Combust. Flame 125 (2001) 778–787.
[10] K.C. Oh, H.D. Shin, J. Mech. Sci Technol. (KSME Int. J.) 19 (11) (2005) 2068–2076.
[11] K.C. Oh, H.D. Shin, Fuel 85 (2006) 615–624.
[12] H. Guo, G.J. Smallwood, Combust. Sci. Technol. 180 (2008) 1695–1708.
[13] J. Appel, H. Bockhorn, M. Frenklach, Combust. Flame 121 (2000) 122–136.
[14] M. Frenklach, Reaction mechanism of soot formation in flames, Phys. Chem. Chem. Phys. 4 (2002) 2028–2037.
[15] M. Abián, A. Millera, R. Bilbao, M.U. Alzueta, Fuel 91 (2012) 307–312.
[16] P.D. Teini, D.M.A. Karwat, A. Atreya, Combust. Flame 159 (2012) 1090–1099.
[17] A.E. Karataş, Ö.L. Gülder, Prog. Energy Combust. Sci. 38 (2012) 818–845.
[18] T.L. Berry Yelverton, W.L. Roberts, Combust. Sci. Technol. 180 (2008) 1334–1346.
[19] T.L. Berry Yelverton, W.L. Roberts, Exp. Thermal Fluid Sci. 33 (2008) 17–22.
[20] H.I. Joo, Ö.L. Gülder, Combust. Flame 158 (2011) 416–422.
[21] R.K. Abhinavam Kailasanathan, T.L.B. Yelverton, T. Fang, W.L. Roberts, Combust. Flame 160 (2013) 656–670.
[22] R.K. Abhinavam Kailasanathan, E.K. Book, T. Fang, W.L. Roberts, Proc. Combust. Inst. 34 (2013) 1035–1043.
[23] R.K. Abhinavam Kailasanathan, J. Zhang, T. Fang, W.L. Roberts, Combust. Sci. Technol. 186 (2014) 815–828.
[24] A.E. Karataş, Ö.L. Gülder, Soot formation in laminar diffusion flames of diluted ethylene in air at pressures up to 20 atm, AIAA Paper AIAA-2014-0652, 2014.
[25] A.E. Karataş, High-pressure soot formation and diffusion flame extinction characteristics of gaseous and liquid fuels, Ph.D Thesis, University of Toronto, 2014. <http://attow.utias.utoronto.ca/~ogulder/karatasPhD2014.pdf>.
[26] K.A. Thomson, Ö.L. Gülder, E.J. Weckman, R.A. Fraser, G.J. Smallwood, D.R. Snelling, Combust. Flame 140 (2005) 222–232.
[27] D.S. Bento, K.A. Thomson, Ö.L. Gülder, Combust. Flame 145 (2006) 765–778.
[28] H.I. Joo, Ö.L. Gülder, Proc. Combust. Inst. 32 (2009) 769–775.
[29] I.M. Miller, H.G. Maahs, High-Pressure Flame System for Pollution Studies with Results for Methane-Air Diffusion Flames, NASA TN D-8407, 1977.
[30] R.L. Axelbaum, C.K. Law, Proc. Combust. Inst. 23 (1991) 1517–1523.
[31] J.H. Kent, H.G.G. Wagner, Proc. Combust. Inst. 20 (1984) 1007–1015.
[32] D.R. Snelling, K.A. Thomson, G.J. Smallwood, Ö.L. Gülder, E.J. Weckman, R.A. Fraser, AIAA J. 40 (2002) 1789–1795.
[33] C.J. Dasch, Appl. Opt. 31 (1992) 1146–1152.
[34] K.A. Thomson, Soot Formation in Annular Non-Premixed Laminar Flames of Methane-Air at Pressures of 0.1 to 4.0 MPa, PhD thesis, University of Waterloo, Waterloo, Canada, 2004.
[35] F. Liu, K.A. Thomson, G.J. Smallwood, Combust. Flame 160 (2013) 1693–1705.
[36] Q. Zhang, H. Guo, F. Liu, G.J. Smallwood, M.J. Thomson, Proc. Combust. Inst. 32 (2009) 761–768.
[37] Q. Zhang, H. Guo, F. Liu, G.J. Smallwood, M.J. Thomson, Combust. Theory Model. 12 (2008) 621–641.
[38] F. Liu, X. He, X. Ma, Q. Zhang, M.J. Thomson, H. Guo, G.J. Smallwood, S. Shuai, J. Wang, Combust. Flame 158 (2011) 547–563.
[39] F. Liu, G.J. Smallwood, JQSRT 84 (2004) 465–475.
[40] J.Z. Wen, M.J. Thomson, M.F. Lightstone, S.N. Rogak, Energy Fuels 20 (2006) 547–559.
[41] S.B. Dworkin, Q. Zhang, M.J. Thomson, N.A. Slavinskaya, U. Riedel, Combust. Flame 158 (2011) 1682–1695.
[42] N.A. Slavinskaya, P. Frank, Combust. Flame 156 (2009) 1705–1722.
[43] F. Liu, S.B. Dworkin, M.J. Thomson, G.J. Smallwood, Combust. Sci. Technol. 184 (2012) 966–979.
[44] F. Liu, K.A. Thomson, H. Guo, G.J. Smallwood, Combust. Flame 146 (2006) 456–471.
[45] M.R.J. Charest, C.P.T. Groth, Ö.L. Gülder, Combust. Flame 158 (2011) 1933–1945.
[46] L.L. McCrain, W.L. Roberts, Combust. Flame 140 (2005) 60–69.
[47] C.S. McEnally, L.D. Pfefferle, Combust. Sci. Technol. 151 (2000) 133–155.
[48] P.M. Mandatori, Ö.L. Gülder, Proc. Combust. Inst. 33 (2011) 577–584.
[49] H. Guo, Z. Gu, K.A. Thomson, G.J. Smallwood, F.F. Baksh, Proc. Combust. Inst. 34 (2013) 1795–1802.